

Review

Boron Nitride-Based Nanomaterials: Synthesis and Application in Rechargeable Batteries

Srikanth Mateti *, Irin Sultana, Ying Chen *, Manikantan Kota and Md Mokhlesur Rahman *

Institute for Frontier Materials, Deakin University, Waurn Ponds, Geelong, VIC 3216, Australia; i.sultana@deakin.edu.au (I.S.); manikantan.kota@pluss.co.in (M.K.)

* Correspondence: s.mateti@deakin.edu.au (S.M.); ian.chen@deakin.edu.au (Y.C.); m.rahan@deakin.edu.au (M.M.R.)

Abstract: Conventional boron nitride material is a resistant refractory compound of boron and nitrogen with various crystalline forms. The hexagonal form, which corresponds to graphite, is used as a lubricant and an additive to cosmetic products because of its higher stability and softness. Recently, various nanostructured boron nitride materials, including nanosheets, nanotubes, nanoparticles, and nanocomposites with diverse new properties, have been achieved through the development of advanced synthesis techniques as well as a deeper understanding of the properties and related applications. As nanostructured boron nitride materials exhibit high chemical, thermal and mechanical stability, the incorporation of nanostructured boron nitride materials into the key components (electrolytes, separators, and electrodes) of electrochemical systems can alleviate various inherent problems. This review article systematically summarizes the integration of nanostructured boron nitride into electrolytes, separators, and electrodes of lithium-ion, sodium-ion, and lithium-sulfur batteries. Various structures, synthesis methods, properties, and electrochemical performance of nanostructured boron nitride incorporated electrolytes, separators, and electrodes in rechargeable batteries are discussed. The challenges and possibilities for future application of boron nitride-based nanomaterials in electrochemical energy storage systems are also highlighted.



Citation: Mateti, S.; Sultana, I.; Chen, Y.; Kota, M.; Rahman, M.M. Boron Nitride-Based Nanomaterials: Synthesis and Application in Rechargeable Batteries. *Batteries* **2023**, *9*, 344. <https://doi.org/10.3390/batteries9070344>

Academic Editor: Yu-Sheng Su

Received: 16 May 2023

Revised: 16 June 2023

Accepted: 16 June 2023

Published: 27 June 2023



Copyright: © 2023 by the authors. Licensee MDPI, Basel, Switzerland. This article is an open access article distributed under the terms and conditions of the Creative Commons Attribution (CC BY) license (<https://creativecommons.org/licenses/by/4.0/>).

1. Introduction

Enhancing battery technologies, predominantly rechargeable batteries (lithium-ion, sodium-ion, and lithium-sulfur), is of high-level importance because the world needs the advancement of electric-powered devices, tools, and vehicles for their decarbonization. Therefore, rechargeable batteries are critical to power a wide range of electronic devices, digital technologies, and electric vehicles with high performance in terms of high energy density, long cycle life, high safety, and low cost [1,2]. To date, enormous attempts have been made, and many problems with rechargeable batteries have already been solved by a combination of nanotechnology and nanomaterials engineering. However, several challenges still exist with rechargeable batteries to be considered. For example, lithium-ion batteries (LIBs) dominate the current market of energy storage technologies, but the device still suffers from low energy density, short life span, high cost, and low safety [3]. On the other hand, low sulfur content in the cathode composition, the formation of dendrite, and the development of an unstable SEI layer are common problems in achieving high-performance lithium-sulfur (Li-S) batteries [4,5]. It is expected that sodium-ion batteries (SIBs) could face many significant issues due to their infancy stage of development. However, all abovementioned rechargeable batteries are fabricated by a combination of three basic elements, such as electrode material (cathode and anode electrodes), electrolyte, and separator. As electrodes, separators, and electrolytes play a key role in the functioning of

the batteries, any development of these three components can contribute to boosting the performance of devices.

To address those issues with rechargeable batteries, many strategies, designs, and materials with new structures have been developed to achieve high-performance batteries. Among various materials developed, nanostructured boron nitride (BN) is supposed to be a very exceptional material with many promising properties. Nanostructured BN materials can be considered in different types, including 0D (zero dimensional, e.g., nanospheres), 1D (one-dimensional, e.g., nanoribbons, nanofibers, and nanotubes), 2D (two-dimensional, e.g., nanosheets and thin films), and 3D (three-dimensional, e.g., nanostructured porous composites) nanostructures. Low dimensional BN materials provide some unique physical and chemical properties, such as high thermal and chemical stability, superb electric insulation, and wide band gap (~5.5 eV) compared to bulk BN materials [6,7]. Thus, nanostructured BN shows great potential for diverse applications. However, the applications of nanostructured BN in energy storage devices are not as common as other materials.

To date, a considerable quantity of research on battery technologies regarding both fundamental and practical studies has been demonstrated. Many important issues (such as high cost, low power/energy density, low capacity, poor safety, and short life cycle) related to the components of these technologies have been partially solved by developing various advanced nano structured materials (such as graphene, MXenes, oxide nanorods/nanofibers etc.) [2,8–11]. Like other advanced materials, the development of nanostructured BN materials with a wide range of properties can play a very important role in alleviating various inherent problems in these existing battery technologies [12]. In this review article, we summarize and discuss the recent progress in various synthesis approaches and properties of nanostructured BN-based materials, design and fabrication of advanced components based on nanostructured BN, and their performance in rechargeable batteries.

2. BN-An Overview

BN has attracted attention in the recent year because of its many delicate functionalities, including transparency to microwaves, low friction coefficient, low density, high thermal conductivity, outstanding resistance to oxidation, and nature of electrical insulation. Researchers are becoming more interested in BN-based materials because of their unique features. BN is a type of synthetic compound that contains an equal amount of B (boron) and N (nitrogen). The B-N bond, with its ionic property, has had a significant impact on the structure of BN allotropes. BN allotropes are capable of forming sp^2 or sp^3 linkage structures [13]. The phase diagram of BN and structural models of various allotropes, including c-BN (cubic-BN), w-BN (wurtzite-BN), h-BN (hexagonal-BN), r-BN (rhombohedral-BN), BNNT (boron nitride nanotubes-single and multiwall), BNNR (boron nitride nanoribbon-zigzag and armchair edges), quantum dots, and boron nitride nanocages, are shown in Figure 1 [14,15]. Figure 1a describes the formation of allotropes over a range of temperatures and pressures. The detailed properties of each type of BN material are also summarized in Table 1.

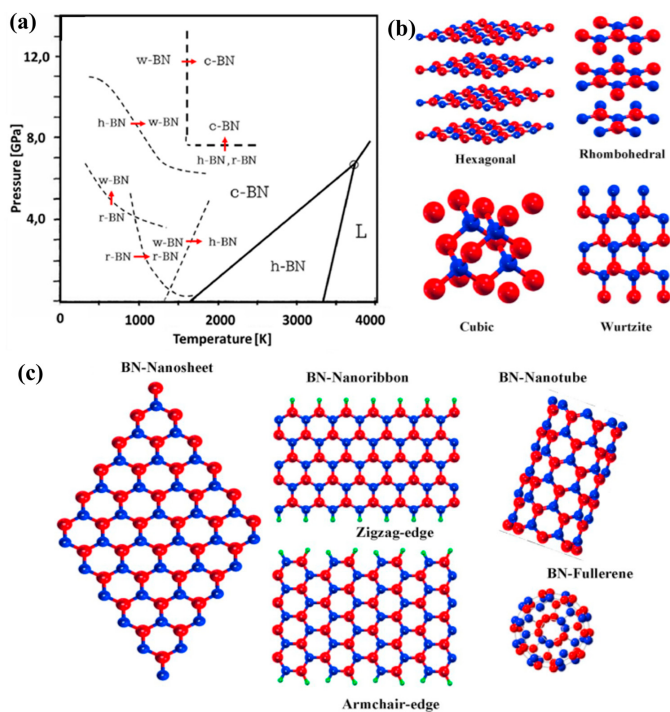


Figure 1. The phase diagram of BN and its various allotropes: (a) Phase diagram of BN, replicated with permission from Elsevier [14]. (b) Various crystal structures of bulk BN, and (c) BN-based nanostructures, replicated with permission from Wiley [15].

Table 1. Properties of different BN allotropes.

Properties	Cubic BN	Wurtzite	Hexagonal	Rhombohedral
Hybridization	sp^3	sp^3	sp^2	sp^2
Crystal structure	Zincblende, analogous to that of diamond. 	Consists of a hexagonal lattice with each ring sitting in a boat configuration. The crystal structure is analogous to that of the rare landslide. 	Structure analogous to that of graphite. 	Each layer of r-BN is the same crystal structure as that of h-BN. However, r-BN follows an ABC stacking configuration whereby boron still sits atop nitrogen atoms, except for layers are offset such that the 1 and 3 atoms (N and N, for example) sit atop the 4 and 6 atoms (B and B in this example) of the ring, below.

Table 1. Cont.

Properties	Cubic BN	Wurtzite	Hexagonal	Rhombohedral
Thermal stability	It has a melting point of approximately 3100 °C, which is higher than that of a diamond.	It can withstand temperatures up to 1400 °C without decomposing.	It has a melting point of approximately 3000 °C, which is still very high and makes it useful for high-temperature applications.	It can withstand temperatures up to 1800 °C without decomposing.
Chemical stability	Inert	Inert	Inert	Inert

3. Synthesis and Properties of Nanostructured BNs

Balmain et al. [16] first synthesized BN in 1842 by reacting H_3BO_3 (molten boric acid) with KCN (potassium cyanide). However, it was not until the early 1960s that the stable form of BN powder was identified. The breakthrough in carbon nanotubes invention in 1991 has initiated research, both theoretical and experimental, on 1D (one dimensional) honeycomb-like structures [17]. Layered BN (h-BN) is one of them, and pure BNNTs were synthesized for the first time in 1995 [18]. Many other 1D BN nanomaterials, including nanorods, nanofibers, and nanowires, were fabricated later. The discovery of graphene in 2004 and subsequent advancements in research on single and multi-layered graphitic nanosheets triggered interest in the field of 2D (two dimension) BN counterparts [19,20]. As a result, nano meshes like h-BN nanosheets and 2D free-standing BN flakes, were created [21]. Synthesis methods of various nanostructured BN are briefly described in this section.

3.1. Boron Nitride Nanosheets (BNNSs)

Mechanical cleavage is reported as the first technique to achieve atomic sheets of BN. To separate graphene monolayers, the mechanical cleavage technique was adopted in 2004. The same method was implemented and successfully produced a variety of other layered materials, which include BN, $NbSe_2$, and MoS_2 [19]. Shear forces, rather than direct pulling pressures via peeling, are used in the mechanical exfoliation of BN. The weak van der Waals bonding between adjacent BN layers was minimized due to pulling force during mechanical peeling, leaving the highly sp^2 -linked in-plane structure intact with a comparable impact from shear force. In 2011, BNNSs were created from a BN powder under N_2 environment by adopting a mild wet ball-milling process with tender shear powers, in which a milling agent of $C_{14}H_{12}O_2$ (benzyl benzoate) was used to reduce ball impacts and processing defilement [22]. An edge hydroxylation of BNNSs has also been carried out. Reactive ball milling is used to produce high-purity and large quantities of BNNSs (Figure 2b). This method is a solvent-free and single-step method to produce various nanosheets of different layered materials [23]. Lee et al. [24] have developed a hydroxide-assisted ball milling procedure that can exfoliate bulk h-BN powders and functionalize BN at the same time (Figure 2c). In this strategy, NaOH solution was used to functionalize and cut h-BN sheets across a response between OH ions and h-BN in which high-speed balls generated shear force exfoliated materials. The oxygen content was increased up to 6.4 at% with OH-BNNS products, which shows that in-plane B locales (other than the edges) had been partially hydroxylated. As a result, the obtained OH-BNNSs decline the water vapor and oxygen permeability of a polymer matrix by 34% and 46%, respectively.

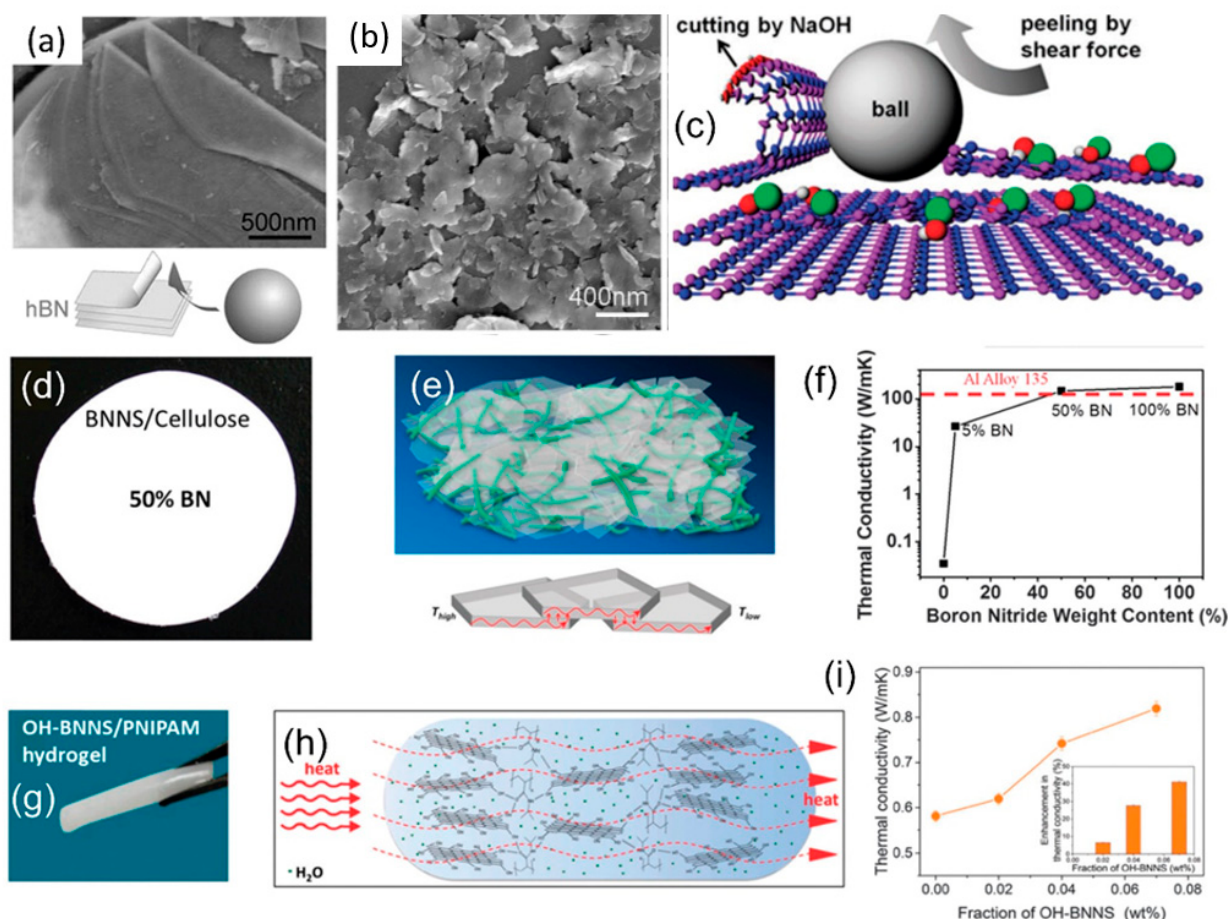


Figure 2. (a) SEM images BN produced from the ball milling process, repeated with permission from RSC [22]. (b) SEM images of BN nanosheets produced using ball milling under reactive gases, repeated with permission from Nature Springer [23]. (c) Preparation and band structures of edge-hydroxylated BN nanosheets (BNNSSs), repeated with permission from [24]. (d,e) Image of BNNS-loaded nano fibrillated cellulose composite with 50 wt% BN its thermal conducting pathways along the plane direction. (f) Thermal conductivity vs BN content in BN/NFC composite, reproduced with permission from [25]. (g,h) Photograph of OH-BNNS filled poly (N-isopropylacrylamide) hydrogel (OH-BNNS/PNIPAM) and thermal conductivity pathway. (i) Improvement of thermal conductivity with increasing the ratio of OH-BNNS, reproduced with permission from [26].

A composite of BNNSSs/cellulose paper loaded with 50 wt% BN phase exhibits a thermal conductivity of $145.7 \text{ W m}^{-1} \text{ K}^{-1}$, which is much better (4000 times) than bare cellulose and greater than the commercial Al alloy 135 (Figure 2f) [25]. An enhanced ordering of BNNSSs after filtration and mechanical pressing operations, as well as the ability to measure conductivity along the basal plane direction, may be responsible for such extraordinary performance. The production of edge-hydroxylated BNNSSs from h-BN precursor under controlled environment (reaction with steam at high temperatures) is shown to be beneficial as a filler to produce poly-(N-isopropyl-acrylamide) (PNIPAM) hydrogel with improved thermal conductivity by 41% by adding only 0.07 wt% of OH-BNNSSs (Figure 2i) [26].

3.2. Boron Nitride Nanotubes (BNNTs)

In 1995, Chopra et al. [18] successfully synthesized BNNTs by adopting an arc-discharge strategy where BNNTs were produced in a plasma arc-discharge device. As bulk BN cannot be used as an electrode directly (due to its insulating nature), a compressed bar of h-BN was embedded into an empty tungsten (W) cathode, shaping a compound anode.

Basically, a quickly cooled copper anode was used as a cathode. The obtained BNNTs show metallic property because of encapsulated nanoparticles at the tube tip-ends generated from the tungsten (W) cathode. Recently, the BOCVD strategy was used by another group where boron (B) powder and metal oxide were used as the reactants [27]. A mixture of MgO and B powders was packed into a BN crucible and placed at the foot of the vertical induction furnace. The furnace was heated at 1300 °C under argon and reactive ammonia stream with a flow rate of 200 (base) and 300 sccm (top), respectively. Argon-transported upward vapors reacted with NH₃ gas within the lower-temperature furnace zone and produced white-colored pure BNNTs (Figure 3). This strategy assisted in moving forward regarding the bigger production of BNNTs when either SnO or FeO was incorporated into the precursor blends [28].

In another set of experiments, a straightforward chemical reaction of blended N₂ and H₂ gas in ball-milled B-Ni powder at 1025 °C was also examined by Lim et al. [29]. BNNTs with a diameter of 20~40 nm and lengths of ~250 nm were effectively created at a low temperature by adopting this strategy without using any toxic/harmful precursors. Scientists from NASA have also advanced a pressurized vapor/condenser (PVC) method to produce very long and small-diameter BNNTs with high crystallinity without the incorporation of any catalysts into the system [30]. Chen et al. [31] developed a unique method of producing different structures of BNNTs. Boron powder was ball milled for 150 h in ammonia atmosphere, and subsequent annealing at 1000 °C led to produce BNNTs (Figure 3a,b) [31]. Further tuning of the precursor and annealing-atmosphere conditions led to producing high purity bamboo-structured nanotubes as well as nanowires (Figure 3c,d) [32]. Growing BNNTs on various irregular surfaces using boron-based ink is fascinating. Figure 3e shows the process, and BNNTs were grown on steel mesh and steel needle and syringe to use in various applications [33].

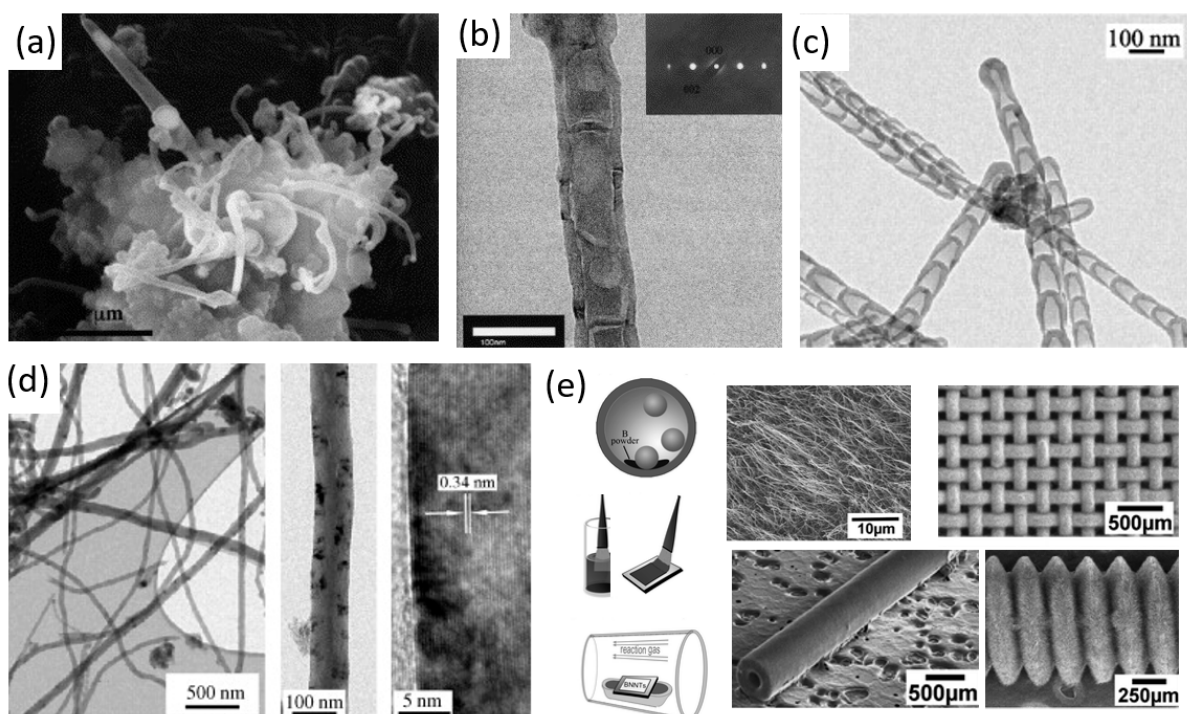


Figure 3. (a,b) SEM and TEM images of grown from ball milled boron subsequent annealing, respectively, produced with permission from Elsevier [31]. (c) SEM image of bamboo shape BNNTs. (d) SEM images of BN rods, produced with permission from Elsevier [32]. (e) B ink produced by ball milling (irregularly shaped objects such as steel mesh, syringe, and screw are used to grow BNNTs), produced with permission from RSC [33].

3.3. Boron Nitride Nanoparticles/Nanopowders (BNNPs)

Fullerenes, nanoparticles, clusters, and nanocapsules are referred to as 0D BN nanocages. BN fullerenes frame skeletal structures comparatively to C₆₀ fullerenes. A high-resolution TEM operated at 300 Kv was used to produce in-situ electron radiation at 20 °C and 490 °C to shape BN fullerenes in 1998. Fullerenes with several layers (six layers) containing 4-, 6-, and 8-membered rings were achieved and can be considered as irradiation derivatives of close-packed agglomerates [34]. Despite fascinating properties, these fullerenes are not investigated largely as compared to C₆₀ because of impractical manufacturing strategies. The spray granulation can be adopted to produce spherical BN particles after being vacuum sintered of h-BN platelets incorporated with a small amount of sodium dodecyl benzenesulfonate (SDBS) in the medium of deionized water [31,35]. The combination of spray drying and pyrolysis is also capable of delivering BN nanoparticles with high dispersibility in which a blend of boric acid/urea is used as a quickly drying agent. A direct reaction between boric acid and ammonium chloride in the presence of copper (II) oxide produces BN nanoparticles with high dispersibility in water is recognized as a straightforward synthesis strategy [36].

3.4. Boron Nitride Nanocomposites (BNNCs)

Various conventional fillers, including Si₃N₄, AlN, and BN, microparticles, show great potential to improve the thermal conductivity of standard polymer materials. The polymers embedded either in graphene or other conductive fillers could increase dielectric constants as well as thermal conductivities before the percolation threshold, whereas the electrical current spillage is not desired [37]. To compensate for such disadvantages, the utilization of electrically insulated BN nanosheets is highly effective. The incorporation of BN sheets as 2D fillers into mineral oil provides a steady Newtonian nanofluid property for application in transformers due to the high thermal conductivity of the BN sheets (Figure 4). The obtained nanofluid provides not only additional electrical protection but also a lower melting point than immaculate mineral oil. It is observed that the thermal conductivity of the nanofluids increases with increasing temperature as compared to the mineral oil, demonstrating that BN nanosheets are responsible for this thermal conductivity. Figure 4 displays the improvement of thermal conductivity with the increase in the amount of BNNTs in the mineral oil [38]. On the other hand, BNNTs and BNNNs are functionalized with -OH, -OCOR, -COR, -R bunches, which shows a significant reinforcement of polymer frameworks compared with the only BN nanostructures. In 2006, an interesting work on the utilization of BNNTs for polystyrene enhancement was reported by Zhi et al. [39]. A short time later, Coleman's bunches performed a wide range of works in this field where various fillers based on BN nanostructures, as well as their factionalized derivatives, were developed for diverse polymers, including PNIPAM, PVA, PVB, PMMA, PEVA, PC, PU, PE, and epoxy [24–26,39–42]. Furthermore, BNNNs are used to reinforce polymer films because of their remarkable mechanical properties. For instance, with the addition of 0.3 wt% BNNNs into the polymer, the elastic modulus and strength of the PMMA films were improved by 22% and 11%, respectively. Furthermore, to progress the fracture toughness of ceramic matrix composites, BN nanoplates show great potential. A composite of ZrB₂-SiC composed of a blended mixture of 1D and 2D BN nanomaterials constructed by adopting spark plasma sintering displayed improved fracture toughness by up to ~24.4% at 1 wt.% BN [43]. Table 2 summarizes different synthesis techniques and their impact on the resulting BN structures and properties [44].

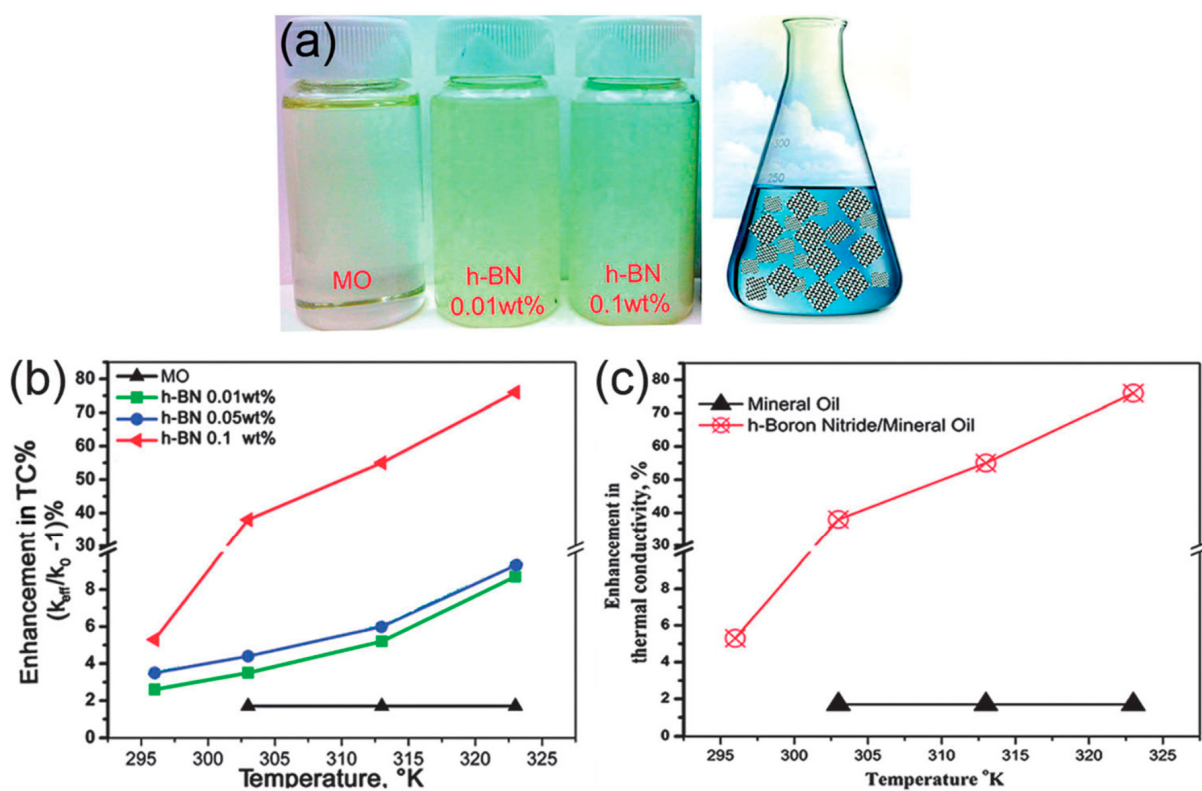


Figure 4. (a) Mineral oil incorporated 0.01 wt.% and 0.1 wt.% BN and a schematic of mineral oil with 2D BNNSs. (b) Thermal conductivity enhancement of various nanofluids with temperatures. (c) The measured thermal conductivity of mineral oil incorporated BNNSs at 323 K, replicated with permission from ACS [38].

Table 2. Summary of different synthesis techniques of h-BN along with necessary post-processing, quality, as well as pros and cons of each method. Reproduced with permission from Wiley [44].

Synthesis Methods	Post-Processing	Final Quality	Pros (+)	Cons (-)
Powder synthesis	Ball milling to thin flakes, liquid phase exfoliation for use in suspensions.	<ul style="list-style-type: none"> Powder of multilayer crystals. Particle sizes from nm to a few tens of μm. 	<ul style="list-style-type: none"> Inexpensive Well-established methods Already at the industrial scale 	<ul style="list-style-type: none"> Small crystallite size. Poor crystalline quality.
High-temperature, high-pressure flux routes	Exfoliation down to the desired thickness.	<ul style="list-style-type: none"> High-quality bulk crystals. Up to mm in width, hundreds of μm thick. Exfoliated flakes (hundreds of μm). 	<ul style="list-style-type: none"> High crystalline quality Relatively thick crystals compared to those produced via deposition methods. Simple B^{10} precursor substitution. 	<ul style="list-style-type: none"> Non-uniform over large areas. Exfoliation is required to produce thin flakes. High pressures are not conducive to large volume production. Higher temperatures incur larger production costs. Long growth time.

Table 2. Cont.

Synthesis Methods	Post-Processing	Final Quality	Pros (+)	Cons (-)
Atmospheric-pressure catalytic flux	Exfoliation down to desired thickness.	<ul style="list-style-type: none"> • High-quality bulk. • Mm scale width, hundreds of μm thick. • Exfoliated flakes (hundreds of μm). 	<ul style="list-style-type: none"> • High crystalline quality • Relatively thick crystals compared to those produced via deposition methods • Atmospheric pressure operating conditions • Simple B^{10} precursor Substitution. 	<ul style="list-style-type: none"> • Non-uniform over large areas. • Exfoliation required to produce thin flakes. • Higher temperatures incur larger production costs. • Long growth time.
Molecular beam epitaxy (MBE)	Transfer to desired substrate if necessary.	<ul style="list-style-type: none"> • High-quality crystal after annealing. • Thin film (mono- to few-layer). • Film area limited to size of substrate. 	<ul style="list-style-type: none"> • High-quality thin film. • High level of molecular control 	<ul style="list-style-type: none"> • Requires ultra-high vacuum conditions. • Thickness limited to a few Layers. • High cost of equipment.
Chemical vapor deposition (CVD) and other deposition methods	Transfer to desired substrate if necessary.	<ul style="list-style-type: none"> • Polycrystalline film. • Films monolayer to tens of micron thick. • Films are limited only by the size of substrate. 	<ul style="list-style-type: none"> • Large area films, good uniformity. • Cheap easily accessible equipment. • Short growth times. 	<ul style="list-style-type: none"> • Grown film is often polycrystalline • Limited control of stacking order.

4. Applications

The application values of materials depend on the properties of materials used. Bulk BN does not have any suitable properties for application in battery technologies. However, BN-derived nanostructured materials (ranging from 0D to 3D structures) including BNNSs, BNNTs, BNNPs, and BNNCs, exhibit outstanding physical and chemical properties, including high thermal and chemical stabilities, as well as distinctive electronic properties. For example, the original BN cannot be used as an active electrode material due to the lack of conductivity. The incorporation of suitable amounts of conductive agents (such as graphene, reduced graphene oxide, graphite, and carbon) makes this material very conductive. On the other hand, the functionalization of nanostructured BN with negatively/positively charged ions through vacancy, doping, compositing, and other techniques produces a certain attraction/repulsion effect on Li^+ / Na^+ / S_x^{2-} ions. Hence, the modification of conventional separators/electrolytes by integration of functionalized nanostructured BN is very effective in attracting ions or repulse ions, which can accelerate the charge diffusion kinetics as well as inhibit polysulfide migration, which may improve the overall electrochemical performance of the batteries. In addition, the integration of a small amount of nanostructured BN into conventional battery materials could prevent unwanted side reactions, short circuits, and dendrites growth because of the excellent thermal conductivity, chemical inertness, and high mechanical strength of the nanostructured BN. As a result, battery cells can operate under extreme environments with improved safety and longer cycle life. The obtained properties through nanostructuring of bulk BN can potentially help to solve many problems related to the battery materials.

5. Applications in LIBs

5.1. Electrolytes for LIBs

It is a serious and challenging issue to operate LIBs in severe environments, especially at elevated temperatures and currents, due to safety issues because of the risk of batteries catching fire and explosion. Electrolytes are one of the responsible components in this regard. Basically, low boiling points of highly flammable organic solvents are commonly used in commercial electrolytes, which increases the internal pressure of the battery cells at elevated temperatures. As a result, the obtained pressure leads to the breakdown of electrode materials and packaging as well. In addition, operation of the LIB cells at high rates also increases the internal temperature of the cells because of thermal dissipations, favoring the occurrence of thermal runaway and failure of the cells [45,46]. From the safety point of view, ionic liquid (IL) based electrolytes are considered the most suitable electrolytes because of their insignificant vapor pressure, high thermal stability, and nonflammability at all temperatures before they decompose [47–50]. However, as a solvent, IL shows strong ionic nature, which decreases lithium-ion transference numbers, strongly limiting the application. In addition, IL is very expensive to use. As an alternative to sole IL electrolyte, Rodrigues et al. [51] developed an advanced electrolyte by a combination of h-BN and IL, which exhibits commendable ionic conductivity with enhanced electrochemical and thermal stability. The obtained h-BN-based composite electrolyte allows LIB cells (both anode and cathode) to operate at high-temperature ranges of 120 °C and 150 °C, respectively (Figure 5a–c). It is also demonstrated that the attained electrochemical performance of h-BN-based composite electrolyte is comparable with conventional organic electrolytes. This work builds a solid starting point that the incorporation of h-BN into IL can develop stable battery systems with high-temperature stability. A more robust electrolyte system of ion gel electrolyte with enhanced Li⁺ transport properties has recently been reported by Kim et al. [52]. In this work, amine functionalized BNNs were incorporated into ion gel electrolytes by adopting in situ thermal polymerization between ionic liquid electrolyte (ILE) and amine-functionalized BNNs (Figure 5d–i). The strong interaction between functionalized BNNs and bis(trifluoromethanesulfonyl) imide (TFSI⁻) anions enhances the lithium transference number and Li⁺ mobility of the ion gel electrolyte. An improved ionic conductivity of 6.47×10^{-4} S cm⁻¹ with a higher t_{Li^+} of 0.23 at 25 °C is realized with the optimized electrolyte. A LiFePO₄ | Li cell with amine-functionalized BNNs-gel electrolyte delivers stable lithium deposition and exceptional battery performance as compared to the cell without amine-functionalized BNNs-gel electrolyte (Figure 5g–i). The obtained findings are critical to advancing more robust solid-state electrolytes to achieve all solid-state batteries with high energy density and safety.

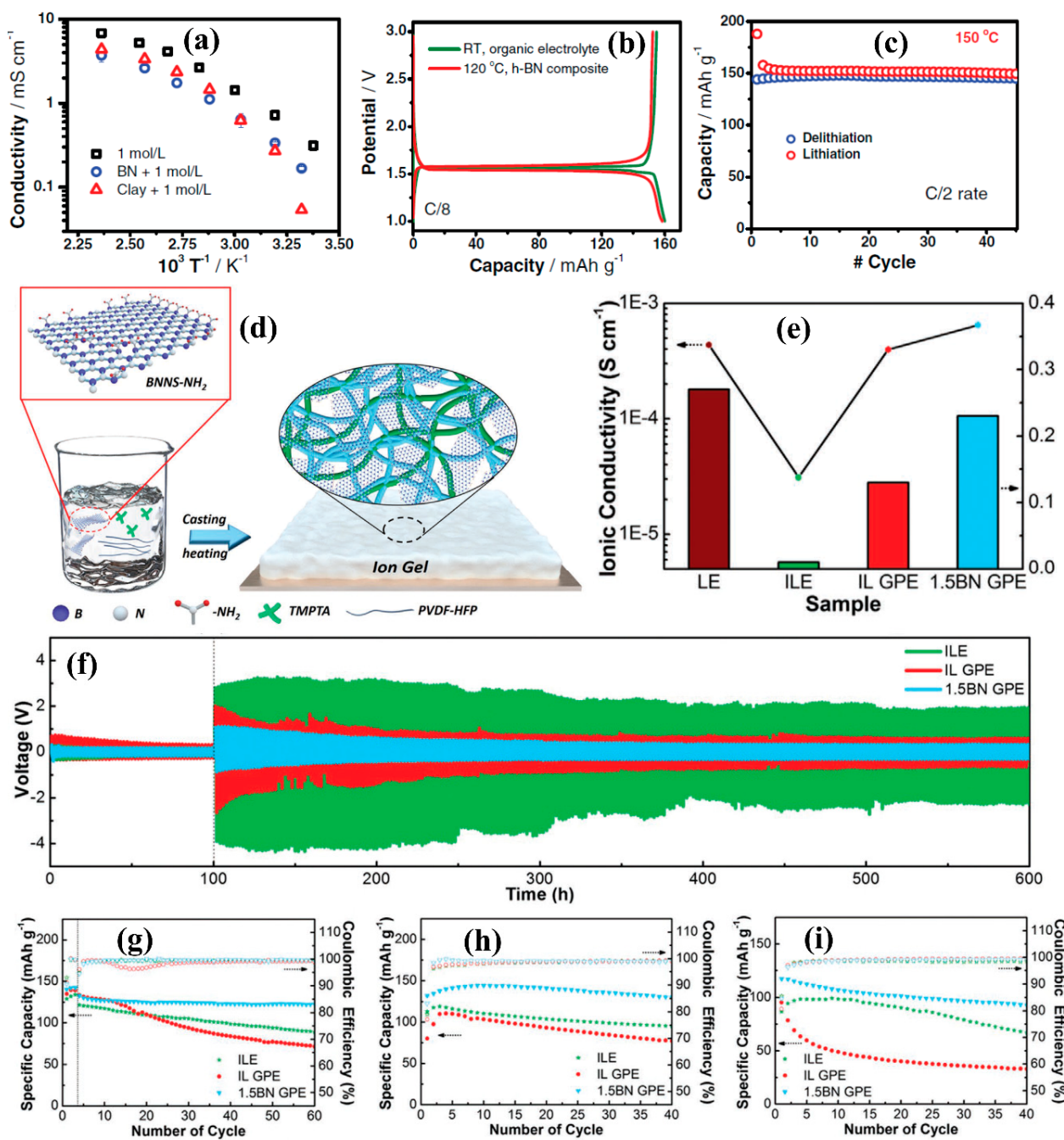


Figure 5. (a–c) Characterization of h-BN incorporated composite electrolyte (Wiley [51], Copied with permission). (a) Ionic conductivity (Arrhenius plot). (b) Comparison between galvanostatic charge-discharge of LTO ($\text{Li}_4\text{Ti}_5\text{O}_{12}$) half-cells with h-BN composite electrolyte cycled at 120 °C and LTO ($\text{Li}_4\text{Ti}_5\text{O}_{12}$) half-cells with conventional electrolyte cycled at 23 °C. (c) Stability performance of the LTO half-cell with h-BN composite electrolyte cycled at 150 °C. (d–i) Characterization of amine-functionalized BNNs-gel electrolyte, reproduced with permission from Wiley [52]. (d) Preparation of amine-functionalized BNNs based ion gel electrolyte (schematic illustration). Li $^{+}$ transport and ionic conductivity of electrolytes (ILE, IL GPE (gel polymer electrolyte)), amine-functionalized BNNs based GPE at 25 °C. (f) Cyclic stabilities of Li symmetric cell with ILE, IL GPE, and 1.5BN GPE at 0.1 mA cm $^{-2}$ current. (g–i) Cyclic stability and Coulombic efficiency of (g) LFP | Li cell. (h) NCM | Li cell. (i) LCO | Li cell with ILE, IL GPE, and 1.5BN GPE as the electrolytes at a current density of 0.2 mA cm $^{-2}$.

5.2. Separators for LIBs

The application of Li metal as anode in battery technology is seriously hampered by two key hurdles: (i) Growth of Li dendrite and (ii) low Coulombic efficiency. Hence, protected and durable Li metal anodes are required for their efficient application in battery technology. Modifying the separator is considered one of the effective approaches to achieve a safe and stable Li metal anode [53–55]. Most previous research focuses on coating commercial separators using different ceramic and organic materials. In 2015, Luo et al. [56] modified a commercial separator by coating it with thermally conductive BNNTs. The obtained BNNTs separator was compatible with organic carbonate-based electrolyte and delivered a commendable Coulombic efficiency of 92%, whereas it was 88% with a pristine separator under the same testing conditions. Later, Rahman et al. [3] developed a BNNTs separator where a conventional polyolefin separator was modified using long and fine BNNTs (Figure 6a–g). In this study, Li^+ ion diffusion channels in the separator were not blocked due to the utilization of long and fine BNNTs, which is critical to achieving a high-performance separator. Additionally, BNNTs show heat dissipation and flame retardation properties. Such important properties of the BNNTs suggest that BNNTs can be considered (compared to other nano materials) very suitable high-performance safe inorganic nanomaterials for the modification of conventional separators to operate battery cells under extreme environments. This BNNT separator exhibits improved thermal stability up to 150 °C, ensuring the safe operation of LIB cells at elevated temperatures. LiFePO₄/Li cells were fabricated using this BNNT separator and tested at various current densities and elevated environment temperatures (50 °C and 70 °C). The cells with BNNT separators perform very well with different current rates and can operate normally at 50 °C and 70 °C (Figure 6f,g), suggesting that the BNNT separator with double side coating is capable of surviving under high current and high temperature because BNNTs absorb additional heat and propagate it through BNNTs during the cycling process. It is clearly seen from Figure 6f,g that a commercial PP separator is incapable of working under the same testing conditions.

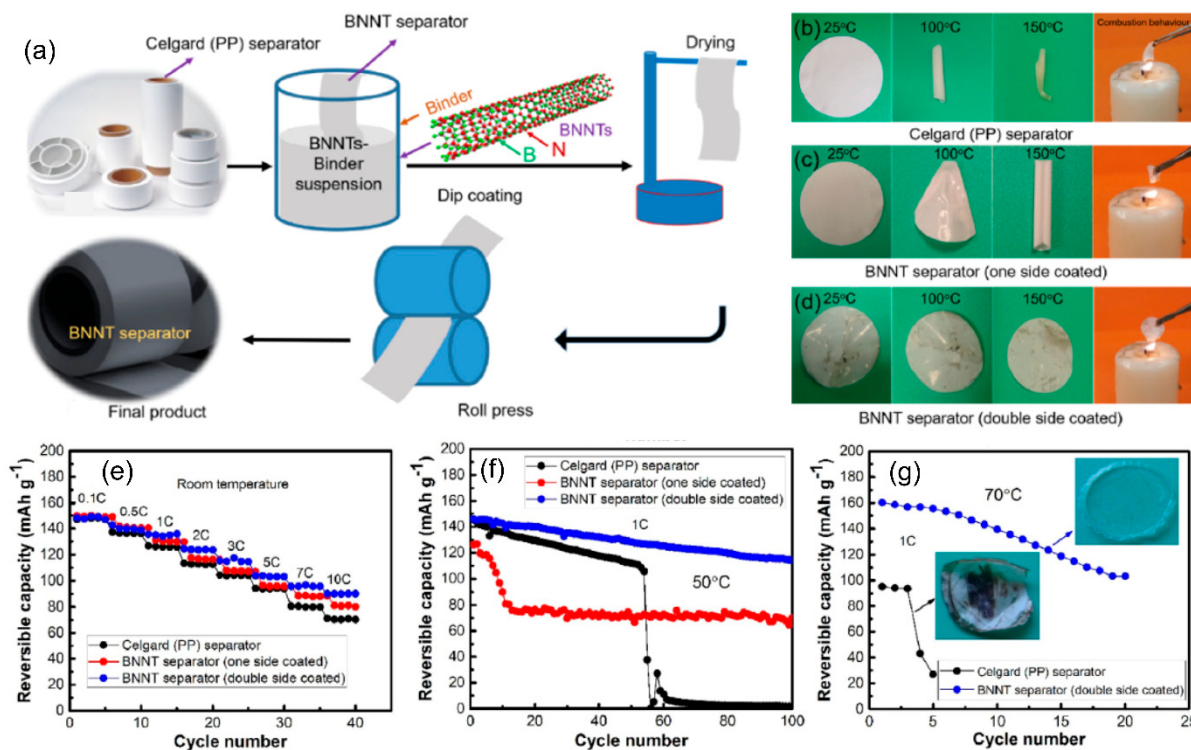


Figure 6. Cont.

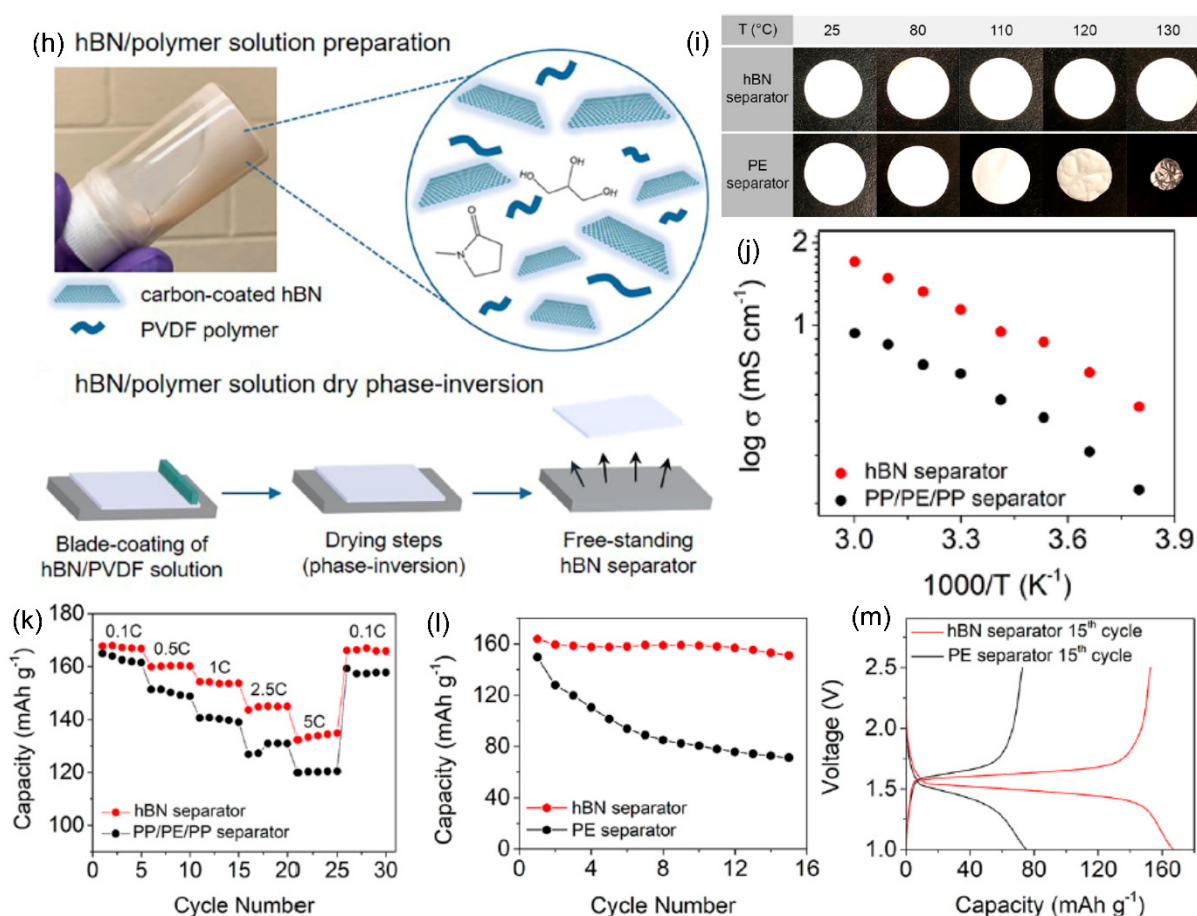


Figure 6. (a–g) Characterization of BNNT separator, copied with authorization from Elsevier [3]. (a) Schematic illustration for the fabrication process of BNNT separator. (b–d) Thermal shrinkage behavior from 25 to 150 °C temperature as well as combustion behavior: (b) Commercial separator (Celgard-PP). (c) One side coated-BNNT separator. (d) Double side coated-BNNT separator. (e–g) Electrochemical performance comparison among different separators: (e) Rate capability at various current densities. (f) Cycling at 50 °C at 1C. (g) Cycling at elevated temperature (70 °C) at 1C. (h–m) Characterization of h-BN nanosheet composite separator (reproduced with permission from ACS [57]). (h) Schematic illustration for the h-BN nanosheet composite separator preparation process. (i) Comparison of thermal properties between h-BN separator and commercial polyolefin-based separator. (j) Ionic conductivity comparison between two separators (h-BN and commercial polyolefin). (k–m) Electrochemical performance evaluation of the h-BN separator with LTO | Li half-cells: (k) Performance of rate capability at different rates with 1.0 M LiPF₆ electrolytes. (i,m) Cycling performance and voltage profiles at 0.2C and 120 °C with LiTFSI in EMIM-TFSI ionic liquid as the electrolyte.

Recently, a carbon-coated h-BN nanosheet-based phase-inversion composite separator has been developed [57]. The obtained h-BN nanosheet composite separator exhibits improved ionic conductivity and enough porosity (compared to the conventional polyolefin separators) to boost battery performance, including rate capability and cycle life (Figure 6h–m). The incorporation of h-BN nanosheet provides high thermal stability to the separator, allowing effective operation of LIB cells at an extreme temperature of 120 °C (Figure 6l,m).

5.3. Electrodes for LIBs

BN is not a suitable material for application as an anode electrode in rechargeable batteries because of its insulating nature. However, a wide range of techniques/strategies, such as vacancy, doping, defect, and compositing, can be adopted to make this mate-

rial conductive [58–60]. In 2013, Lei et al. [60] successfully synthesized a few layers (2–6 atomic layers) of carbon-doped boron nitrides (BCNs) in the form of nanosheets and used them as LIB anode for the first time (Figure 7a–d). Surprisingly, such a structure shows promising Li^+ storage performance. The obtained capacity was 390 mAh g^{-1} at 30 mA g^{-1} current after 100 cycles. Even more promising electrochemical performance of stable capacity of $\sim 100 \text{ mAh g}^{-1}$ at 2 A g^{-1} after 5000 cycles was achieved. This work demonstrates a significant advance in designing boron nitride-based light elements anode materials for rechargeable batteries. A sheet-like anode composed of h-BN chemically integrated with silicon carbonitride (SiCN) prepared by the pyrolysis route is also reported as a high-performance LIB anode [61], as shown in Figure 7e–g. The composite anode of SiCN/BN delivers commendable electrochemical performance with a charge capacity of $\sim 517 \text{ mAh g}^{-1}$ at 100 mA g^{-1} and $\sim 283 \text{ mAh g}^{-1}$ at 2400 mA g^{-1} , respectively. The addition of a moderate amount ($\sim 10 \text{ wt \%}$) of BN to polysilazane and subsequent carbon coating of the SiCN phase through pyrolysis are responsible for such high electrochemical due to improved electrical conductivity. Basically, the incorporation of BN into anode electrode materials has a significant impact in terms of capacity, stability, and safety.

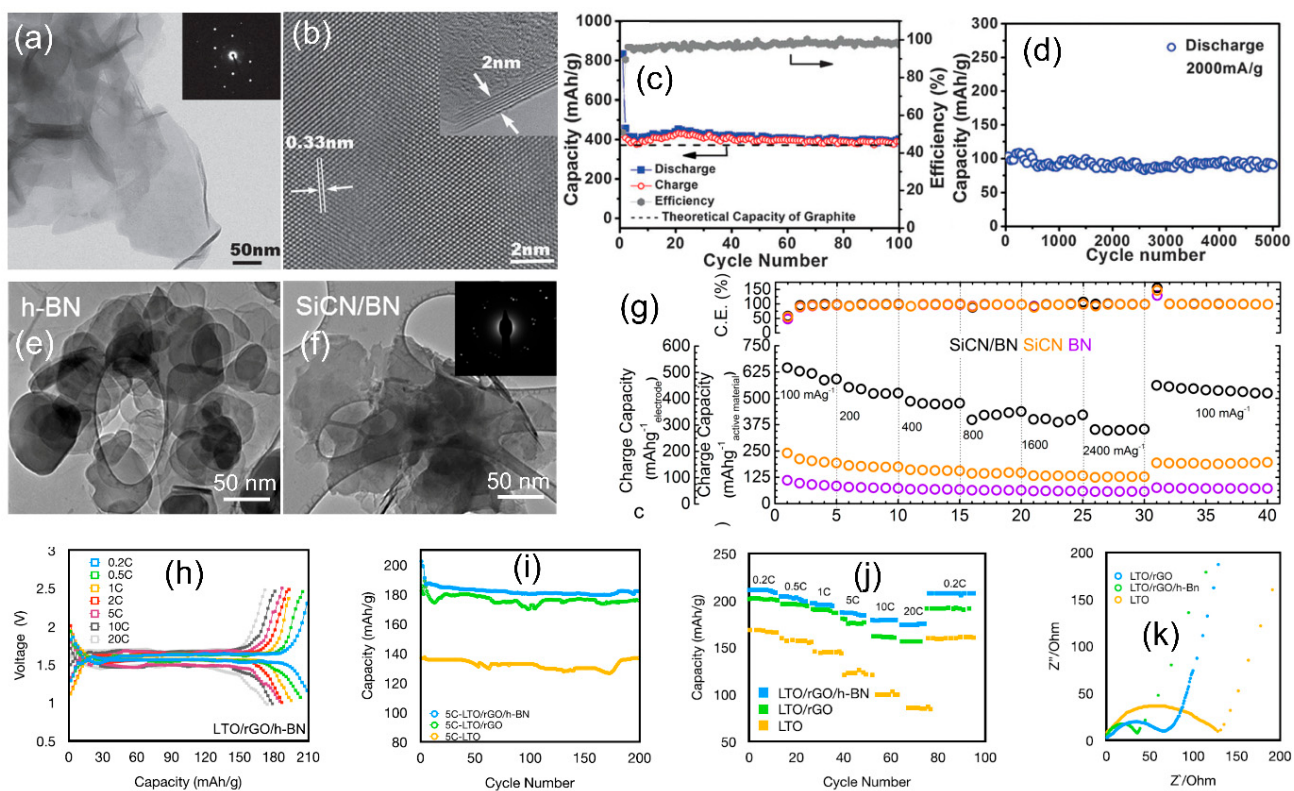


Figure 7. (a–d) Characterization of carbon doped boron nitrides (BCNs) nanosheets (copied with permission from RSC [60]). (a) Bright-field TEM image and SAED pattern (inset) of the nanosheets. (b) HRTEM images of a nanosheet an edge folding (inset). (c) Cyclic stability and Coulombic efficiency performance at 30 mA g^{-1} current for 100 cycles. (d) Cyclic performance of the BCN nanosheet (few-layers) electrode at 2 A g^{-1} current. (e–g) Characterization of SiCN/BN composite anode (reproduced with permission from ACS [61]). (e) TEM image of as-obtained BN sheets. (f) As-synthesized SiCN/BN composite material (inset shows the SAED pattern). (g) Electrochemical performance and comparison. (h–k) Electrochemical performance evaluation (reproduced with permission from AIP [62]). (h) Charge-discharge curve at different rates of LTO/r-GO/h-BN electrode. (i) Cycling stability comparison among different electrodes. (j) Rate capability comparison among different electrodes. (k) electrochemical impedance analysis.

The well-known lithium titanium oxide (LTO) anode still faces many drawbacks (such as poor intrinsic conductivity and narrow electrochemical window) when compared to commercial anodes (graphite). Although extensive research has overcome many problems with LTO materials through the incorporation of r-GO (reduced graphene oxide), the strategies still show fast capacity decay at a higher current density of above 5C because of high internal resistance. Recently, an effective strategy has been executed to achieve three-dimensional frameworks of LTO with the incorporation of r-GO and h-BN [62] (Figure 7h–k). The obtained LTO/r-GO/h-BN composite electrode is capable of showing typical discharge-charge curves with perfect shape even when operated at a very high current of 20C (Figure 7h). The LTO/r-GO/h-BN electrodes have a higher capacity and better stability, as well as rate capability, than other electrodes (Figure 7i,j). It is clearly demonstrated that the modified electrodes (LTO/r-GO/h-BN) show lower impedance than LTO and LTO/r-GO electrodes, suggesting efficient ionic diffusion through (LTO/r-GO/h-BN) electrode (Figure 7k). Such structure permits much better electron transport, Li⁺ storage, and ion diffusion as well. To achieve optimum performance, the loading ratio of h-BN is very critical to be considered. A facile microwave irradiation technique (MWI) has also been reported to prepare Co₃O₄/r-GO/h-BN nanocomposite, which has the potential to be used as high-temperature anode [63]. Both the specific surface area and thermal stability of the Co₃O₄/r-GO are enhanced significantly due to the addition of h-BN. As a result, the Co₃O₄/r-GO/h-BN nanocomposite anode demonstrates outstanding cyclic stability with 100% capacity retention operated at high temperatures.

6. Applications in SIBs

The utilization of electrode materials incorporated with BN in SIBs is hardly reported. This research is in its early stage, and it is currently limited to the theoretical investigation. Recently, several DFT (density functional theory) investigations have been carried out on BN-based materials. In 2017, Nejati et al. [64] studied the interaction of Na (both atomic and cationic) with BNNTs (zigzag single-walled with various diameters) and BNNSs. It was demonstrated that Na adsorption leads the highest occupied molecular orbital (HOMO) to shift from the surface of BN sheet and (5, 0) BNNT on the Na atom, suggesting energy destabilization (Figure 8a,b). The interaction between surfaces and Na⁺ is much greater than the adsorption value, and the atomic Na was strictly associated with the diameter of BNNTs. The interaction between the surfaces and the Na⁺ is triggered by the static electricity during hybridization. However, V_{cell} of the SIB cell could increase if the structural curvature of BN was reduced. To determine the V_{cell}, the interaction between Na⁺ and the BN surface can be considered the key factor. The reduction of the curvature of BN nanostructures is beneficial to increase the p-character and aromaticity of the hybridization of B atoms and decrease the interaction with atomic Na. By decreasing the curvature, the V_{cell} of the SIB cell is increased by 1.12 V for BN (5, 0) nanotube and 1.55 V for BNNS, respectively, suggesting the potential application of BNNS as an anode in SIBs.

A new strategy has been introduced to increase the performance of BNNSs [65]. This DFT study demonstrates that replacing some N atoms with P atoms can improve the performance of the BNNSs, whereas it is decreased if B atoms are partially replaced by larger Al atoms (Figure 8c,d). The electronic properties of BNNSs are affected seriously due to the adsorption of both Na⁺ and Na on the doped BN nanosheet. The ΔE of the cell and V_{cell} is significantly increased after replacement. The replacement of three N atoms of the hexagonal ring of BN with larger P atoms increases the adsorption energy of Na⁺, leading to a significant improvement of the ΔE of the cell and V_{cell}, respectively. This DFT study provides guides to develop high-performance BNNSs anode for SIBs. A new graphene like 2D material of Si₂BN has also been investigated as a probable anode for SIBs. DFT calculation determines that the planar Si₂BN materials exhibit buckled structure when adsorption of Na⁺ takes place. Such transition delivers a superior specific capacity of 993.0 mAh g⁻¹, suggesting a potential high-performance anode for SIBs [66]. Recently, Bao et al. [67] have explored the potential of using blue phosphorene (blue-P) and h-BN as

anode with high theoretical specific capacities of 801 and 541 mAh g^{-1} and low diffusion barriers 0.08 and 0.07 eV for LIBs and SIBs, respectively. The energy barriers of 0.26 eV for Li and 0.15 eV for Na are calculated along the $\text{I}_4 \rightarrow \text{I}_4$ path (Figure 8e). Such properties suggest that the BN/P can potentially be used as an ideal anode candidate for SIBs.

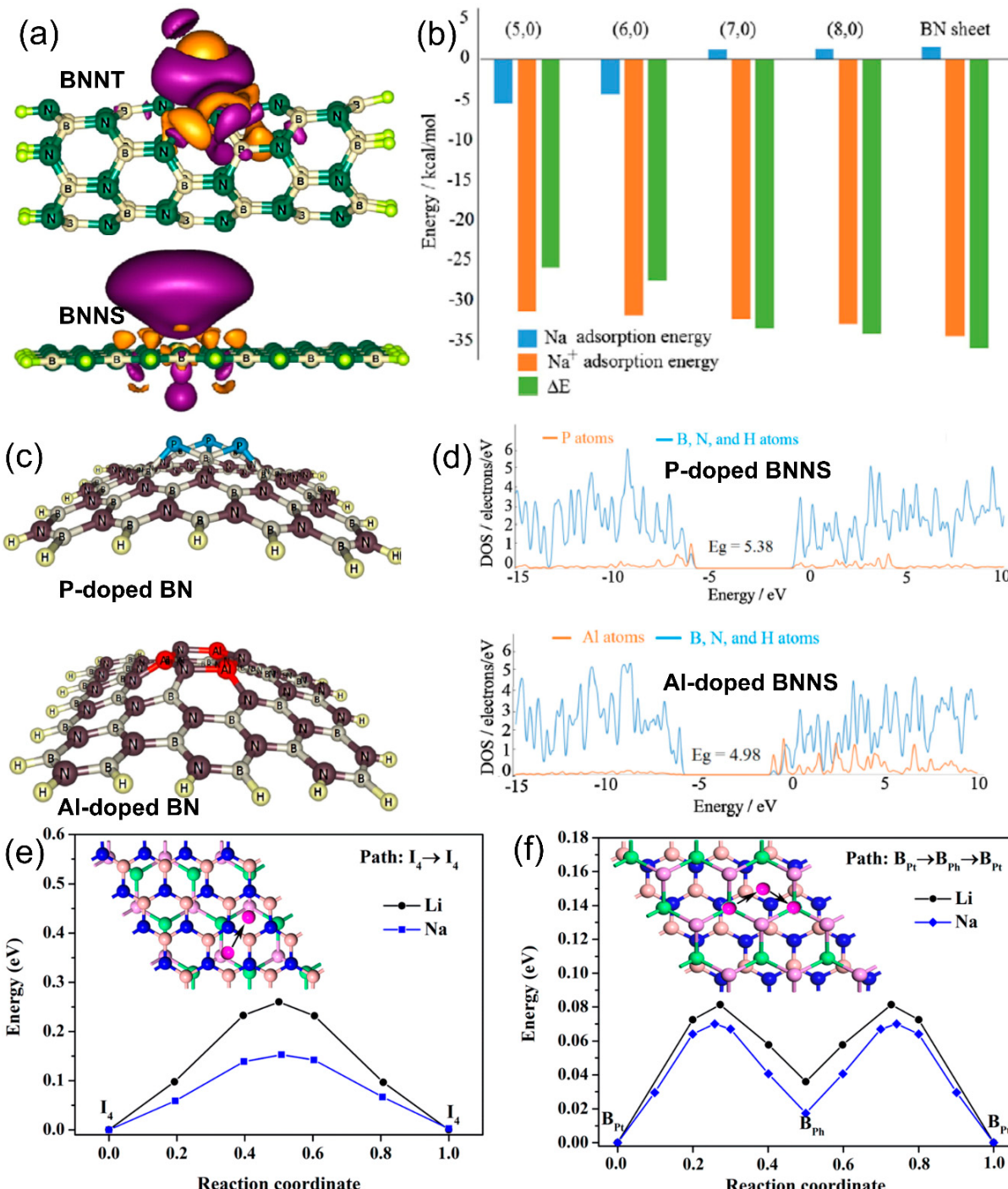


Figure 8. (a,b) LUMO profiles (Na-BNNT (5,0) and Na-BNNS) and Na/Na⁺ adsorption energies on BNNT and BNNS (replicated with permission from Elsevier [64]). (c,d) Unit cell structures (optimized) P and Al-doped BNNSs and Partial DOS plots of P and Al-doped BNNSs (reproduced with permission from Elsevier [65]). (e,f) Diffusion path and the corresponding energy profiles: (e) Path $\text{I}_4 \rightarrow \text{I}_4$ in h-BN/M (Li or Na)/blue-phosphorene (BN/M/P). (f) Path $\text{B}_{\text{Pt}} \rightarrow \text{B}_{\text{Ph}} \rightarrow \text{B}_{\text{Pt}}$ in BN/P/M (reproduced with permission from ACS [67]).

7. Applications in Li-S

Among currently available battery technologies, Li-S (lithium-sulfur) batteries are considered the most appealing applicants to serve as the batteries of the next generation with excellent electrochemical performance. The electrochemical reaction of $16\text{Li} + \text{S}_8 \rightarrow 8\text{Li}_2\text{S}$ delivers a high specific capacity of 1675 mAh g^{-1} as well as a high energy density of 2600 Wh kg^{-1} [68]. However, several problems, such as lithium dendrites formation and growth and the dissolution of intermediate products in electrolytes formed during the cycling process (known as the shuttle effect), still exist in these devices. As a result, rigorous capacity fading (poor cycling stability), as well as low Coulombic efficiency, are realized with these devices [69,70], which has delayed their efficient practical application. To solve these issues, many strategies have been suggested where BN-based materials are used to create superior architecture of the components, as discussed below.

7.1. Separator for Li-S

To avoid shuttle effect, separator modification by incorporating many materials, such as black phosphorus, metal-organic framework, graphene oxide, and different metal oxides (such as Al_2O_3 and TiO_2), has already been tested [71–75]. Despite the success of separator modification to inhibit the PS shuttle effect, the transport of electrons and the movement of Li^+ are seriously hampered by these separators, providing unsatisfactory sulfur utilization and rate capability. To achieve highly stable Li-S batteries, a pioneering initiative was carried out by Kim et al. [76]. In this study, a very effective multifunctional membrane of BN-carbon separator was fabricated, which powerfully inhibits the shuttling of polysulfides, leading to the impressive electrochemical properties of the Li-S cells (Figure 9a–c). The combination of a BN layer and a carbon layer was used in this separator, and it guards the Li anode against sudden side reactions to accelerate battery performance, which includes high Coulombic efficiency, long cycle life, and stable capacity. The obtained BN-carbon separator provides three advantages, including (i) effective suppression of polysulfides, (ii) smooth electron transfer pathway due to carbon layer, and (iii) uniform thermal distribution due to BN layer, which is responsible for the improved electrochemical properties of the Li-S cell.

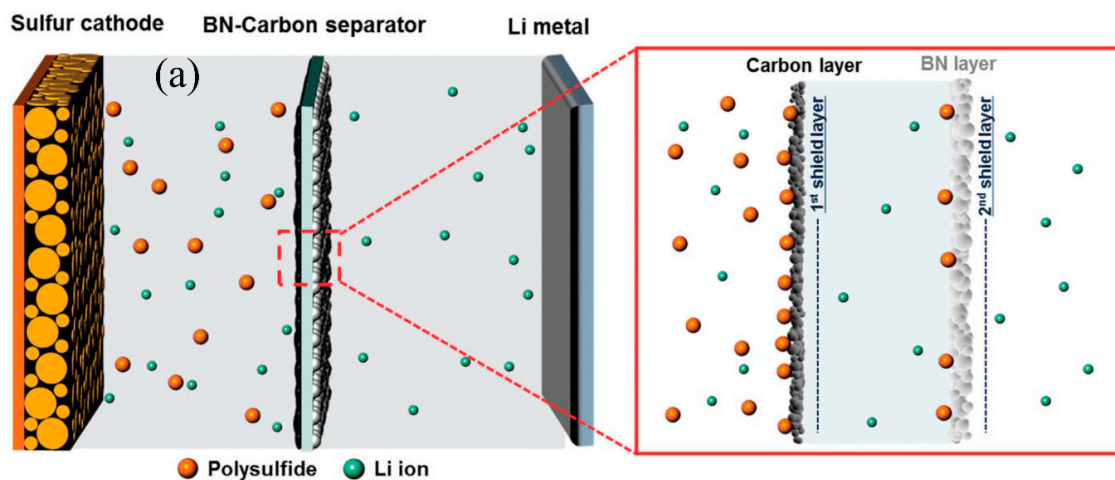


Figure 9. *Cont.*

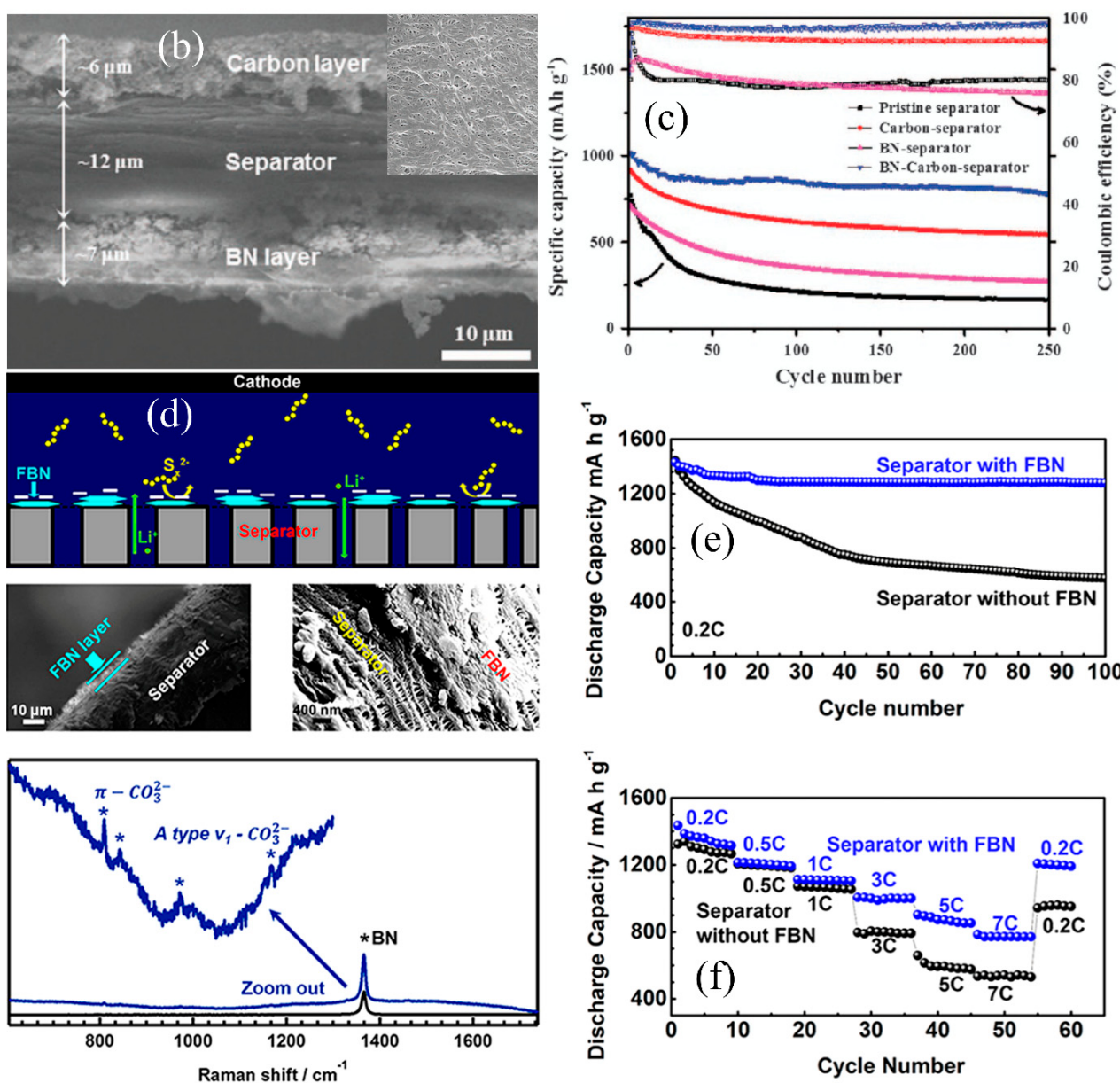


Figure 9. (a–c) Characterization of BN-carbon separator (reproduced with permission from Nature Springer [76]). (a) Schematic presentation of the function of BN-carbon separator during cycling. (b) SEM image (carbon, separator, and BN layers (inset shows a pristine separator)). (c) Electrochemical performance comparison at 0.5C among different separators. (d–f) Characterization of functionalized BN (FBN) separator (replicated with permission from ACS [77]). (d) Schematic visual of the Li-S cell constructed with FBN separator, SEM images (cross-section of the coating layer and FBN separator surface), and Raman spectrum of FBN nanosheets. (e,f) Battery performance of (e) Cyclic test of two cells (with and without FBN separator) at 0.2C up to 100 cycles. (f) Rate capability performance of the cells (with and without FBN).

In 2019, Fan et al. [77] also developed a multifunctional separator. Functionalized BNNSs with negatively charged groups were integrated into a commercial Celgard separator (Figure 9d–f). The obtained separator is capable of eliminating the shuttle effect, improving electron transport speed and Li^+ diffusion rate as well. It was revealed that the obtained BN separator can limit dissolved polysulfides (PSs) migration through the separator due to the strong electrostatic interaction between functionalized boron nitride (FBN) nanosheets and negatively charged PSs products, which limits the migration of the dissolved polysulfides (PSs) through a separator. As a result, high electrochemical perfor-

mance (such as high-rate capability, long-term cyclic stability, and high specific capacity) of the cell is realized. The strategy of the modification of the commercial Celgard separator with FBN nanosheets has the potential to develop high-performance Li-S batteries. Recently, Kim et al. [78] have developed a purified BNNT-based separator, which is capable of facilitating the transfer of ions through the separator, alleviating the shuttle effect at the cathode, and protecting the Li metal anode from dendrite formation. In this study, a conventional polypropylene (PP) separator was modified by incorporating a suitable amount of purified BNNT in which a 3-dimensional (3D) spider net-like structure was formed on PP separator by randomly stacking one-dimensional (1D) purified BNNT materials. The ionic conductivity and diffusion coefficient of this modified separator were much better than those of PP separator. As a result, Li-S cells with a purified BNNT separator exhibit greater performance (such as power and gravimetric energy density) than Li-S cells with other separators [78].

7.2. Interlayer/Interface for Li-S Batteries

To block the movement of the products of polysulfides produced by the sulphur cathode to the metallic Li anode as well as to absorb soluble polysulfides, the addition of an additional interlayer between the sulfur cathode and the separator is recognized as a very practical approach to achieve high-performance Li-S batteries with excellent rate capability and stable cycle life. However, the performance of the interlayer depends on the materials used. Carbon-based interlayers [79], such as conductive MWCNT (multiwalled carbon nanotube) films, polyvinylidene fluoride/carbon nanofiber composite membranes, graphene films, nanoporous carbon cloth coated with Al_2O_3 , Fe_3C /carbon nanofiber webs, microporous carbon papers, carbon fiber cloth, TiO_2 /graphene films, and porous CoS_2 /carbon papers, etc., are commonly used. Although interlayer enhances the performance of Li-S cells substantially, however, interlayer preparation with enough conductivity as well as appropriate thickness and light weight are critical for the devices. Therefore, the development of lightweight interlayers with high conductivity as well as proper thickness is a challenge. Among various materials, BN-based materials, especially BNNS, have an excellent possibility for the manufacture of interlayer with lightweight to develop high-performance Li-S batteries. Fan et al. [80] first planned and fabricated an interlayer with light-weight by integration of graphene and FBN nanosheets thin film on the cathode side (Figure 10a–d). The obtained interlayer provides very distinct properties, which include electrostatic interaction originating from positively and negatively charged groups of BN nanosheets and PS products, respectively, as well as high conductivity and flexibility due to the incorporation of graphene. As a result, this interlayer can reduce charge transfer resistance and capture PS on the cathode surface significantly, providing outstanding cyclic stability compared to the cells without such interlayer. The cells with this interlayer exhibit very low-capacity degeneration rate of 0.0067% at 1C and 0.0037% at 3C per cycle up to 1000 cycles, respectively (Figure 10c).

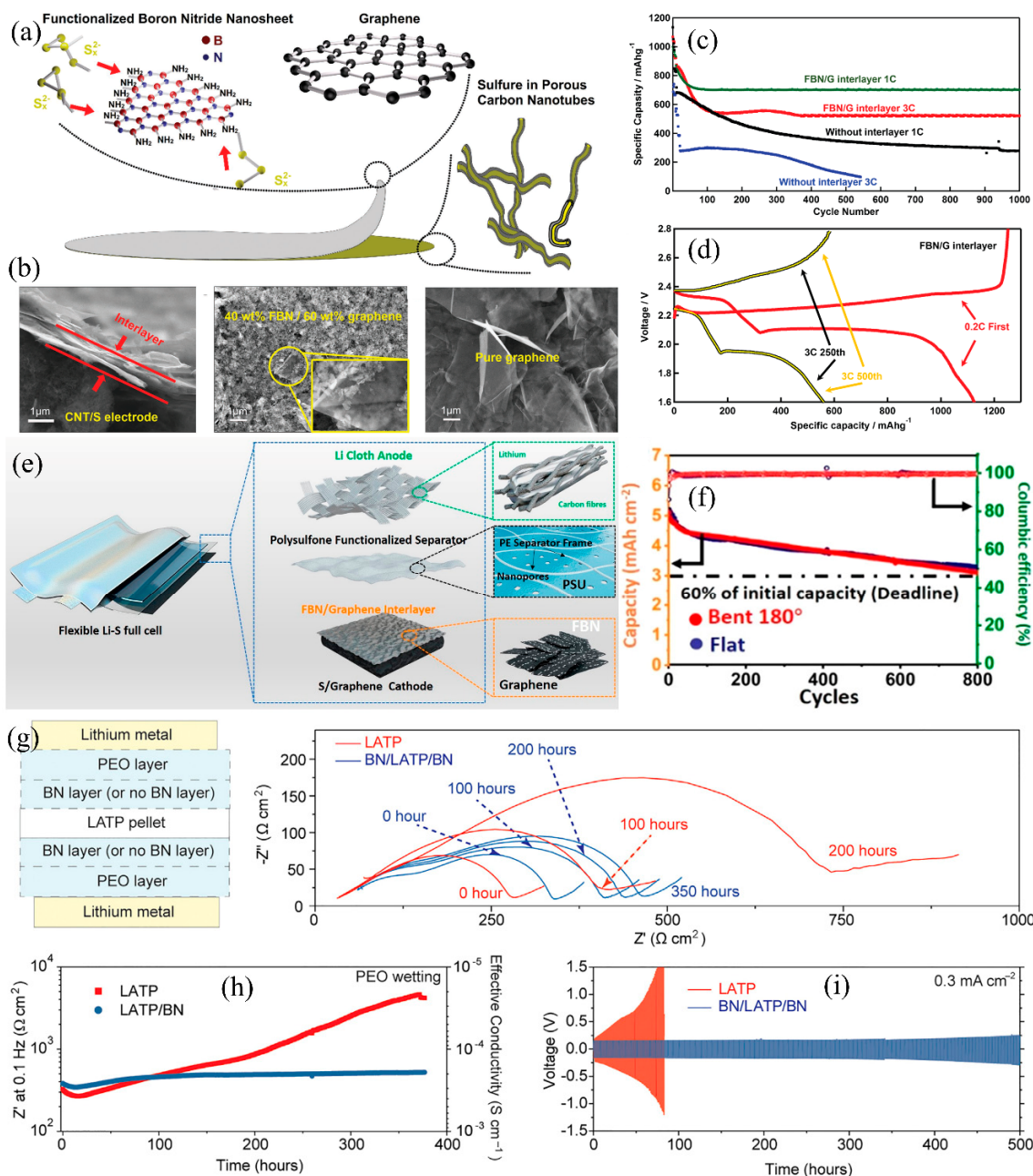


Figure 10. (a–d) Characterization of functionalized boron nitride (FBN) nanosheets/graphene (G) interlayer (replicated from [80] with permission from Wiley). (a) Schematic illustration of the interlayer of FBN/G. (b) SEM image: FBN/G interlayer (cross-section) and cathode. (c,d) Electrochemical performance of Li-S cells: (c) Cyclic performance of the cells with an interlayer of FBN/G and without an interlayer at current densities of 1C and 3C. (d) Corresponding charge-discharge curves with FBN/G interlayer for the selected cycles. (e,f) Characterization of Li-S full cells (reproduced with permission from [81] ACS). (e) Schematic model of the fabrication of flexible Li-S full cells composed of anodes (lithium cloth), separators (PSU-Celgard), and free-standing graphene/sulfur cathodes protected by FBN/G interlayers. (f) Flat and bent state performance (cyclic stability and Coulombic efficiency) of the Li-S pouch cells. (g–i) Evaluation of the Li/Li symmetric cells assembled with $\text{Li}_{1.3}\text{Al}_{0.3}\text{Ti}_{1.7}(\text{PO}_4)_3$ (LATP) and LATP/BN pellets (replicated from [82] with permission from Joule). (g) The schematic presentation and the Nyquist plots of Li/Li symmetric cells with PEO infiltrating. (h) Impedance measurement of Li/Li cells (bare LATP and LATP/BN pellets where 1–2 μm thick PEO was added on each side to wet the interface). (i) Cyclic stability (long-term) performance of the cells with bare LATP (red) and LATP/BN (blue) operated at 0.3 mA cm^{-2} current at 60°C .

A very flexible Li-S battery fabricated with anode of lithium cloth, interlayer of functionalized BN nanosheets/graphene, separator of functionalized polysulfone, and cathode of graphene/sulfur composite has also been developed recently (Figure 10e,f) [81]. In this study, a molten lithium infusion process is adopted to construct lithium cloth anodes where molten lithium was stored in the micro/nanopore of functionalized carbon cloth. The flexibility and stability of the lithium cloth electrodes originate from the 3D hierarchical nanostructured networks on the carbon cloth. The integration of functionalized BN nanosheets/graphene interlayers and functionalized-polysulfone separators creates a synergistic effect which powerfully inhibits the shuttle of the PSs. As a result, the obtained flexible Li-S full-cells demonstrate commendable electrochemical performance in terms of high areal capacity (5.13 mAh cm^{-2}) and high volumetric and gravimetric energy densities (468 Wh L^{-1}) up to 800 cycles in the folded state (Figure 10f). This research opens an opportunity to develop practical flexible Li-S batteries with energy density. Boron nitride nanocomposite coating has also been developed to stabilize the interface of solid electrolyte/anode in lithium-metal batteries [82]. The obtained coating delivers some unique properties (such as electronically insulating and ionically conductive, as well as chemically and mechanically robust), which impede the reduction of $\text{Li}_{1.3}\text{Al}_{0.3}\text{Ti}_{1.7}(\text{PO}_4)_3$ (LATP) solid electrolyte by the Li metal (Figure 10g–i). The solid-state batteries of $\text{LiFePO}_4/\text{LATP}/\text{BN}/\text{PEO}$ (polyethylene oxide)/Li can retain 96.6% capacity for up to 500 cycles in 70 days. The progression of BN-based coating film shows a significant prospective to broaden the working window of unstable solid electrolytes against Li metal anode.

7.3. Sulfur Cathodes for Li-S Batteries

The combination of active sulfur species and various carbon-based nanomaterials is documented as a popular strategy to develop sulfur cathodes with high sulfur loading, high conductivity, and less volumetric expansion. To alleviate the shuttle of sulfur cathode, a perfect structure of carbon/vacancy defects is required to achieve carbon-pore confinements of sulfur and LiPSs (lithium polysulfides) [83–88]. The performance of Li-S batteries with composite sulfur cathodes incorporating BN and carbon is still limited. Basically, vacancy defects BN materials, along with dangling bonds (like carbon materials), may have a great impact on the local electronic structures, and the atoms closer to the vacancies become very reactive and they eventually catalyze the transformation of the LiPSs from Li_2S_6 to Li_2S . Hence, such BN materials with chemical catalysis and physical adsorption properties due to active sites can be very attractive substrates to improve the cyclic stability and Coulombic efficiency of the Li-S batteries. Li et al. [89] introduced a new type of sulfur cathode composed of MWCNTs (multi-walled carbon nanotubes) and BNFs (porous boron nitride fibers) to load a sufficient amount of active sulfur (Figure 11a). This fascinating structural design is highly capable of trapping the active sulfur and assisting in confining the soluble PS within the cathode region, preventing the loss of active material. In this robust structure, porous BNFs trap active material, whereas CNTs deliver a favorably inexpensive and fast conductive corridor for electron transfer, enhancing the structural integrity and conductivity of the cathode structure. The cell with CNTs/BNFs/S cathode shows an attractive electrochemical performance with a specific capacity retention of 627 mAh g^{-1} at 1C after 300 cycles, where the calculated capacity decay was only 0.091% per cycle. In the case of CNTs/S cathode, the specific capacity retention was only 319 mAh g^{-1} . The Coulombic efficiency of CNTs/BNFs/S cathode at 1C was very close to 100% (Figure 11d). Thus, CNTs/BNFs/S cathode could lead to low active sulfur loss with improved cycling stability.

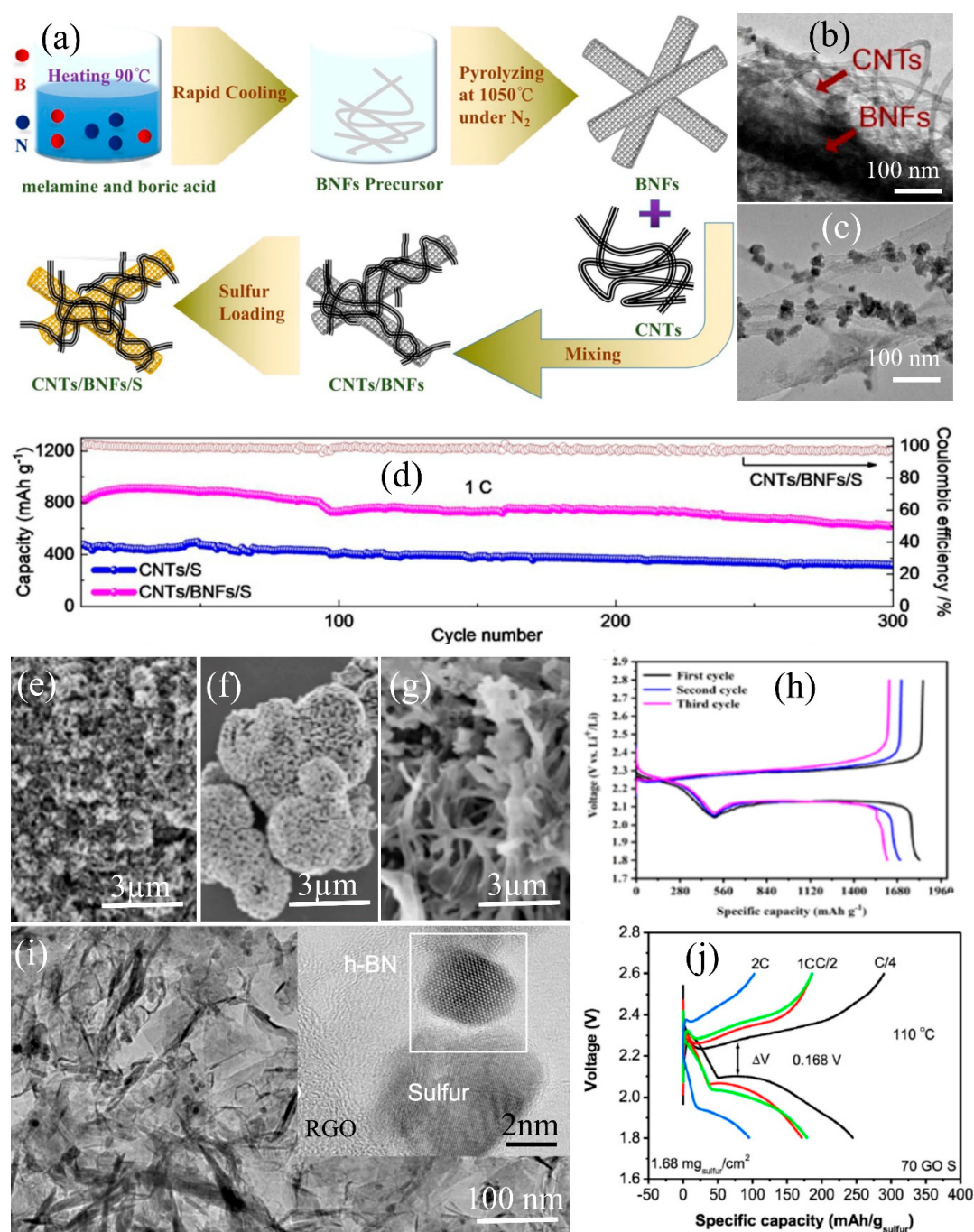


Figure 11. (a–d) Characterization of CNTs-BNFs (carbon nanotubes-boron nitride fibers)-S (sulfur) cathode (replicated with permission from Springer Nature [89]). (a) Schematic illustration of the preparation procedure. (b) TEM image of CNTs and BNFs. (c) TEM image of CNTs/BNFs/S. (d) Cycling stability and Coulombic efficiency obtained at 1C. (e–h) Characterization of boron nitride (BN)-Ketjenblack-xKOH@S composite (replicated with permission from ACS publishers [90]). (e–g) SEM images: (e) Ketjenblack, (f) Ketjenblack-KOH. (g) BN-Ketjenblack-KOH, and (h) discharge-charge cycling (first three cycles) at 0.1C rate of the BN-Ketjenblack-KOH@S composite electrodes. (i,j) Characterization of r-GO/h-BN/S (reduced graphene oxide-hexagonal boron nitride-sulfur) composite (replicated with permission from Springer Nature [91]). (i) TEM bright-field image. HRTEM image is shown in inset, which displays dispersion of sulfur on the edges of r-GO and h-BN flake, and (j) Discharge-charge graphs of the r-GO/h-BN/S (70 wt% GO) composite electrode operated at various current rates.

Another combination of BN-incorporated Ketjenblack-KOH@S has been reported to effectively prevent the PSs migration from cathode to anode [90] (Figure 11e–h). An evaporatively loading sulfur method was applied to construct this composite cathode, where in situ grown BN nanofibers pre-treated by Ketjenblack through 1M KOH chemical etching and high-temperature calcination were used (Figure 11a). In this composite structure, sulfur is anchored with BN nanofibers and Ketjenblack via S-O-B and S-O-C interactions. In addition, sulfur is also infiltrated into the meso/micro pores of BN-Ketjenblack-xKOH substrates. The Li-S cells with this cathode (BN-Ketjenblack-1KOH@S) display a high discharge capacity of $1822.5 \text{ mAh g}^{-1}$ at 0.1C (Figure 11h), which is greater than the theoretical capacity (1675 mAh g^{-1}) of sulfur. Recently, an alternative composite cathode composed of r-GO, h-BN, and sulfur was fabricated by implementing a ball milling process [63] (Figure 11i,j). The optimum ratio of r-GO to h-BN is critical to building high-performance RGO/h-BN/S composite cathodes when compared to GO and h-BN. The incorporation of h-BN into the cathode system improves the functionality of the cells to operate at high temperatures (110°C). The synergistic effect originating from the combined structure of BN/r-GO greatly increases the adsorption capability of PSs, thus managing the cells to deliver outstanding performance at high temperatures.

8. Conclusions and Outlook

Although BN-based nanostructures are recognized as an important class of nanomaterials due to their fascinating properties, the application of nanostructured boron nitride in various energy storage systems is not as common as that of other nanomaterials. Some of the distinctive properties, such as high chemical-thermal-mechanical stability, as well as high insulating in nature, make BN-based nanomaterials very special for specific applications in battery technology. Basically, the properties of various nanostructured BN differ from each other, depending on the synthesis techniques, size, diameter, and shape of the materials. This review systematically demonstrates a broad opportunity for the synthesis of various nanostructured BN-based materials with unique properties, characterization, and efficient applications in battery technologies, including LIBs, SIBs, and Li-S batteries.

Among various synthesis methods, mechanical exfoliation is treated as the basic strategy to produce nanosheets from h-BN powder by adopting the ball milling technique carried out under different environments. BN nanosheets can also be functionalized during ball milling by incorporating various chemical solvents into the milling jars. In contrast, the mechanical milling technique is not very successful in producing BN nanotubes. Basically, arc-discharge strategy/heat treatment of bulk BN powder in a furnace under argon with an NH_3 gas is demonstrated as the most practical method to produce BN nanotubes. Very recently, the PVC (pressurized vapor-condenser) method has been developed to produce very long, greatly crystalline, and small-diameter BNNTs without the utilization of any catalysts. Boron nitride nanoparticles/nano powders can be produced by a combination of spray granulation-vacuum sintering, as well as spray drying-pyrolysis techniques. A straightforward strategy of direct reaction between boric acid and ammonium chloride in the presence of copper (II) oxide can also produce BN nanoparticles. BN nanosheets, BN nanotubes, and their derivatives are broadly utilized as fillers to construct distinctive polymer nanocomposites.

This review also considers the latest development of battery materials (electrolytes, separators, electrodes) through the modification of conventional materials with either nanostructured BN or their derivatives. The addition of functionalized BNNs into IL (ionic liquid) improves the thermal stability and ionic conductivity of the IL, leading LIB cells to operate under high temperatures with improved electrochemical performance. Similarly, the coating of a conventional polypropylene separator with appropriately engineered BNNTs leads to the improved properties of high mechanical and thermal stability, leading to the separators to function in risky situations (high temperature and high current). A conventional separator incorporated with carbon-coated BNNs also increases the thermal stability of the separator with high ionic conductivity, managing efficient operation of the

LIB cells at high temperatures with commendable electrochemical performance. On the other hand, nanostructured BN as an electrode does not have any promising application in LIBs and SIBs because of the inferior conductivity. A blended anode of BN nanostructure/conductive materials (such as carbon or r-GO) improves electrochemical performance in LIBs. Three-dimensional frameworks of the oxide materials with the incorporation of r-GO and h-BN enhance lithium ions diffusion, electron transport, and lithium-ion storage capability of the anodes in LIBs. However, an optimal ratio of the components is critical to achieving robust three-dimensional frameworks with promising electrochemical performance. In contrast, the application of BN materials as an anode in SIBs is just in its infancy stage.

Furthermore, nanostructured BN materials (h-BN, functionalized BNNs, and BNNTs) incorporated commercial separator is very effective in preventing PSs migration through the electrolyte from cathode to anode side in Li-S battery, which enhances electron transport as well as Li^+ diffusion rate, and provides a uniform thermal distribution, delivering much improved electrochemical performance. To minimize the maximum negative effect of PSs migration, an additional BN-based thin interlayer is fabricated and used. Functionalized BNNs are found to be very attractive materials to fabricate robust interlayers with appropriate thickness, high conductivity, and lightweight, which are critical to achieving high-performance Li-S batteries. The recent development of nanostructured BN as sulfur loading substrate has also been discussed in this review. Porous nanostructured BN is recognized as an effective substrate for loading a high amount of sulfur. The appropriate integration of porous nanostructured BN, carbon materials, and sulfur together provides a very special composite architecture of high sulfur-loaded cathode. Such robust sulfur cathode architecture creates a synergistic effect among the components, leading to enhanced electrochemical performance of the Li-S cells.

Although significant progress has been made in the application of nanostructured BN in battery technology, the obtained research findings are still in the early stage but they are an important research topic. To move forward, several challenges related to the synthesis, properties, and applications in batteries need to be solved.

- (i) **Synthesis techniques:** Not many synthesis techniques have been advanced to produce various BN nanomaterials in large quantities. To tune the properties of BN materials, the most advanced synthesis techniques are required. For example, functionalized BNNs or BNNTs are very effective in preventing polysulfide migration in Li-S batteries. To make these materials viable, additional conductive agents, such as graphene or carbon, were incorporated. On the other hand, the nanostructured BN cannot be used directly as an active electrode material for LIBs or SIBs due to the lack of conductivity. Various conductive materials, including graphene, reduced graphene oxide, graphite, and carbon, were used to provide enough conductivity. Thus, advanced strategies or synthesis techniques need to be introduced to achieve conductive BN nanomaterials for direct application in batteries.
- (ii) **Electrolytes and separators:** The shuttle effect is recognized as a crucial task for Li-S batteries to achieve better devices, which is caused by the dissolution of polysulfides in liquid electrolyte and subsequent migration through a separator from cathode to anode and reduction to lower-order polysulfides or sulfides, triggering the active material loss and the passivation of Li anode as well. As a result, this shuttle effect initiates short circuit, leads to self-discharging, and provides low Coulombic efficiency during cycling. Until now, not much research work has been conducted on electrolytes to eliminate the so-called shuttle effect from Li-S batteries completely. In addition, existing electrolytes cannot tackle the shuttle effect due to the lack of required properties, including wide electrochemical stability window, outstanding thermal stability, excellent mechanical strength, reduced interfacial resistance, low electronic conductivity, and high ionic conductivity. An advanced composite solid-state electrolyte incorporating BN nanomaterials with required properties needs to be developed to replace liquid electrolyte in Li-S batteries. In addition, conventional separators in

LIBs/SIBs are unable to survive under very extreme environments, such as high temperatures with high current operation. Although coating with nanostructured BN can improve the thermal stability of conventional separators, smooth ion diffusion through a separator would be a significant challenge to be considered.

- (iii) Electrode/electrolyte interface chemistry: The formation of an unstable SEI layer, as well as the growth of Li dendrites at the Li anode/electrolyte interfaces, create serious safety as well as technological concerns about the practical utilization of Li metal as an anode in Li-ion and Li-S batteries. The formation of Li dendrites initiates many issues, which include electrolyte depletion, increased impedance, capacity fading, self-discharge, as well as active Li anode loss during the cycling process. Even though significant efforts have been made to advance BN-incorporated dendrite-free Li metal anodes, the success is limited due to the lack of understanding of interface chemistry. For a better understanding of interface chemistry at the solid-solid or solid-liquid interface, it is necessary to carry out more research by adopting the most advanced in-situ/ex-situ characterization techniques.
- (iv) Electrodes: Very little has been revealed about the application of BN materials as anodes in LIBs/SIBs as well as sulfur hosts in Li-S batteries. As BN materials suffer from conductivity, the fabrication of nanocomposites/hybrid structures with conductive agents is required. It is a significant challenge but mandatory to design advanced anodes for LIBs/SIBs and advanced sulfur cathodes for Li-S batteries by the incorporation of a wide range of BN nanomaterials with various conductive agents as well as high sulfur content, respectively. High sulfur content could effectively immobilize sulfur at the molecular level in the composite nano structure.

Author Contributions: Conceptualization, S.M. and M.M.R.; writing—original draft preparation, S.M., I.S., M.K. and M.M.R.; writing—review and editing, M.M.R. and Y.C.; supervision, S.M., M.M.R. and Y.C.; project administration, M.M.R. and Y.C.; funding acquisition, S.M., M.M.R. and Y.C. All authors have read and agreed to the published version of the manuscript.

Funding: The authors gratefully thank the Australian Research Council (ARC) for the financial support through Industrial Transformation Research Hub (IH200100035), Discovery Project (DP190102656) and Linkage Project (LP200301537).

Data Availability Statement: Data is available on request.

Conflicts of Interest: The authors declare no conflict of interest.

References

1. Bruce, P.G.; Freunberger, S.A.; Hardwick, L.J.; Tarascon, J.-M. Li–O₂ and Li–S batteries with high energy storage. *Nat. Mater.* **2012**, *11*, 19–29. [[CrossRef](#)]
2. Rahman, M.M.; Sultana, I.; Fan, Y.; Yu, B.; Tao, T.; Hou, C.; Chen, Y. Strategies, design and synthesis of advanced nanostructured electrodes for rechargeable batteries. *Mater. Chem. Front.* **2021**, *5*, 5897–5931. [[CrossRef](#)]
3. Rahman, M.M.; Mateti, S.; Cai, Q.; Sultana, I.; Fan, Y.; Wang, X.; Hou, C.; Chen, Y. High temperature and high rate lithium-ion batteries with boron nitride nanotubes coated polypropylene separators. *Energy Storage Mater.* **2019**, *19*, 352–359. [[CrossRef](#)]
4. Manthiram, A.; Fu, Y.; Chung, S.-H.; Zu, C.; Su, Y.-S. Rechargeable lithium–sulfur batteries. *Chem. Rev.* **2014**, *114*, 11751–11787. [[CrossRef](#)]
5. Li, F.; He, J.; Liu, J.; Wu, M.; Hou, Y.; Wang, H.; Qi, S.; Liu, Q.; Hu, J.; Ma, J. Gradient Solid Electrolyte Interphase and Lithium-Ion Solvation Regulated by Bisfluoroacetamide for Stable Lithium Metal Batteries. *Angew. Chem. Int. Ed.* **2021**, *60*, 6600–6608. [[CrossRef](#)]
6. Emanet, M.; Sen, Ö.; Taşkin, I.Ç.; Çulha, M. Synthesis, functionalization, and bioapplications of two-dimensional boron nitride nanomaterials. *Front. Bioeng. Biotechnol.* **2019**, *7*, 363. [[CrossRef](#)] [[PubMed](#)]
7. Gonzalez Ortiz, D.; Pochat-Bohatier, C.; Cambedouzou, J.; Bechelany, M.; Miele, P. Exfoliation of hexagonal boron nitride (h-BN) in liquid phase by ion intercalation. *Nanomaterials* **2018**, *8*, 716. [[CrossRef](#)] [[PubMed](#)]
8. Ming, F.; Liang, H.; Huang, G.; Bayhan, Z.; Alshareef, H.N. MXenes for rechargeable batteries beyond the lithium-ion. *Adv. Mater.* **2021**, *33*, 2004039. [[CrossRef](#)]
9. Chen, H.; Liu, Q.-Y.; Jing, M.-X.; Chen, F.; Yuan, W.-Y.; Ju, B.-W.; Tu, F.-Y.; Shen, X.-Q.; Qin, S.-B. Improved interface stability and room-temperature performance of solid-state lithium batteries by integrating cathode/electrolyte and graphite coating. *ACS Appl. Mater. Interfaces* **2020**, *12*, 15120–15127. [[CrossRef](#)] [[PubMed](#)]

10. Hu, X.-Y.; Jing, M.-X.; Yang, H.; Liu, Q.-Y.; Chen, F.; Yuan, W.-Y.; Kang, L.; Li, D.-H.; Shen, X.-Q. Enhanced ionic conductivity and lithium dendrite suppression of polymer solid electrolytes by alumina nanorods and interfacial graphite modification. *J. Colloid Interface Sci.* **2021**, *590*, 50–59. [[CrossRef](#)]
11. Jing, M.-X.; Yang, H.; Han, C.; Chen, F.; Yuan, W.-Y.; Ju, B.-W.; Tu, F.-Y.; Shen, X.-Q.; Qin, S.-B. Improving room-temperature electrochemical performance of solid-state lithium battery by using electrospun $\text{La}_2\text{Zr}_2\text{O}_7$ fibers-filled composite solid electrolyte. *Ceram. Int.* **2019**, *45*, 18614–18622. [[CrossRef](#)]
12. Pu, J.; Zhang, K.; Wang, Z.; Li, C.; Zhu, K.; Yao, Y.; Hong, G. Synthesis and modification of boron nitride nanomaterials for electrochemical energy storage: From theory to application. *Adv. Funct. Mater.* **2021**, *31*, 2106315. [[CrossRef](#)]
13. Petrescu, M.; Balint, M.-G. Structure and properties modifications in boron nitride. Part I: Direct polymorphic transformations mechanisms. *UPB Sci. Bull. Ser. B* **2007**, *69*, 35–42.
14. Shayan, A.; Sayed, A.; Mahdi, A.; Farzaneh, S. A comprehensive review on planar boron nitride nanomaterials: From 2D nanosheets towards 0D quantum dots. *Prog. Mater. Sci.* **2022**, *124*, 100884.
15. Arenal, R.; Lopez-Bezanilla, A. Boron nitride materials: An overview from 0D to 3D (nano) structures. *Wiley Interdiscip. Rev. Comput. Mol. Sci.* **2015**, *5*, 299–309. [[CrossRef](#)]
16. Balmain, W. XLVI. Observations on the formation of compounds of boron and silicon with nitrogen and certain metals. *Lond. Edinb. Dublin Philos. Mag. J. Sci.* **1842**, *21*, 270–277. [[CrossRef](#)]
17. Oberlin, A.; Endo, M.; Koyama, T. Filamentous growth of carbon through benzene decomposition. *J. Cryst. Growth* **1976**, *32*, 335–349. [[CrossRef](#)]
18. Chopra, N.G.; Luyken, R.; Cherrey, K.; Crespi, V.H.; Cohen, M.L.; Louie, S.G.; Zettl, A. Boron nitride nanotubes. *Science* **1995**, *269*, 966–967. [[CrossRef](#)]
19. Novoselov, K.S.; Geim, A.K.; Morozov, S.V.; Jiang, D.-E.; Zhang, Y.; Dubonos, S.V.; Grigorieva, I.V.; Firsov, A.A. Electric field effect in atomically thin carbon films. *Science* **2004**, *306*, 666–669. [[CrossRef](#)] [[PubMed](#)]
20. Golberg, D.; Bando, Y.; Huang, Y.; Terao, T.; Mitome, M.; Tang, C.; Zhi, C. Boron nitride nanotubes and nanosheets. *ACS Nano* **2010**, *4*, 2979–2993. [[CrossRef](#)]
21. Corso, M.; Auwarter, W.; Muntwiler, M.; Tamai, A.; Greber, T.; Osterwalder, J. Boron nitride nanomesh. *Science* **2004**, *303*, 217–220. [[CrossRef](#)] [[PubMed](#)]
22. Li, L.H.; Chen, Y.; Behan, G.; Zhang, H.; Petracic, M.; Glushenkov, A.M. Large-scale mechanical peeling of boron nitride nanosheets by low-energy ball milling. *J. Mater. Chem.* **2011**, *21*, 11862–11866. [[CrossRef](#)]
23. Xing, T.; Mateti, S.; Li, L.H.; Ma, F.; Du, A.; Gogotsi, Y.; Chen, Y. Gas protection of two-dimensional nanomaterials from high-energy impacts. *Sci. Rep.* **2016**, *6*, 35532. [[CrossRef](#)]
24. Lee, D.; Lee, B.; Park, K.H.; Ryu, H.J.; Jeon, S.; Hong, S.H. Scalable exfoliation process for highly soluble boron nitride nanoplatelets by hydroxide-assisted ball milling. *Nano Lett.* **2015**, *15*, 1238–1244. [[CrossRef](#)] [[PubMed](#)]
25. Zhu, H.; Li, Y.; Fang, Z.; Xu, J.; Cao, F.; Wan, J.; Preston, C.; Yang, B.; Hu, L. Highly thermally conductive papers with percolative layered boron nitride nanosheets. *ACS Nano* **2014**, *8*, 3606–3613. [[CrossRef](#)]
26. Xiao, F.; Naficy, S.; Casillas, G.; Khan, M.H.; Katkus, T.; Jiang, L.; Liu, H.; Li, H.; Huang, Z. Edge-hydroxylated boron nitride nanosheets as an effective additive to improve the thermal response of hydrogels. *Adv. Mater.* **2015**, *27*, 7196–7203. [[CrossRef](#)]
27. Tang, C.; Bando, Y.; Sato, T.; Kurashima, K. A novel precursor for synthesis of pure boron nitride nanotubes. *Chem. Commun.* **2002**, 1290–1291. [[CrossRef](#)]
28. Zhi, C.; Bando, Y.; Tan, C.; Golberg, D. Effective precursor for high yield synthesis of pure BN nanotubes. *Solid State Commun.* **2005**, *135*, 67–70. [[CrossRef](#)]
29. Lim, S.H.; Luo, J.; Ji, W.; Lin, J. Synthesis of boron nitride nanotubes and its hydrogen uptake. *Catal. Today* **2007**, *120*, 346–350. [[CrossRef](#)]
30. Smith, M.W.; Jordan, K.C.; Park, C.; Kim, J.-W.; Lillehei, P.T.; Crooks, R.; Harrison, J.S. Very long single-and few-walled boron nitride nanotubes via the pressurized vapor/condenser method. *Nanotechnology* **2009**, *20*, 505604. [[CrossRef](#)]
31. Chen, Y.; Gerald, J.F.; Williams, J.; Bulcock, S. Synthesis of boron nitride nanotubes at low temperatures using reactive ball milling. *Chem. Phys. Lett.* **1999**, *299*, 260–264. [[CrossRef](#)]
32. Li, L.; Li, C.P.; Chen, Y. Synthesis of boron nitride nanotubes, bamboos and nanowires. *Phys. E Low-Dimens. Syst. Nanostruct.* **2008**, *40*, 2513–2516. [[CrossRef](#)]
33. Li, L.H.; Chen, Y.; Glushenkov, A.M. Boron nitride nanotube films grown from boron ink painting. *J. Mater. Chem.* **2010**, *20*, 9679–9683. [[CrossRef](#)]
34. Golberg, D.; Bando, Y.; Stéphan, O.; Kurashima, K. Octahedral boron nitride fullerenes formed by electron beam irradiation. *Appl. Phys. Lett.* **1998**, *73*, 2441–2443. [[CrossRef](#)]
35. Han, W.; Ma, Z.; Liu, S.; Ge, C.; Wang, L.; Zhang, X. Highly-dispersible boron nitride nanoparticles by spray drying and pyrolysis. *Ceram. Int.* **2017**, *43*, 10192–10200. [[CrossRef](#)]
36. Xiong, C.; Tu, W. Synthesis of water-dispersible boron nitride nanoparticles. *Eur. J. Inorg. Chem.* **2014**, *2014*, 3010–3015. [[CrossRef](#)]
37. Romasanta, L.J.; Hernández, M.; López-Manchado, M.A.; Verdejo, R. Functionalised graphene sheets as effective high dielectric constant fillers. *Nanoscale Res. Lett.* **2011**, *6*, 508. [[CrossRef](#)]
38. Taha-Tijerina, J.; Narayanan, T.N.; Gao, G.; Rohde, M.; Tsentalovich, D.A.; Pasquali, M.; Ajayan, P.M. Electrically insulating thermal nano-oils using 2D fillers. *ACS Nano* **2012**, *6*, 1214–1220. [[CrossRef](#)]

39. Zhi, C.; Bando, Y.; Tang, C.; Honda, S.; Kuwahara, H.; Golberg, D. Boron nitride nanotubes/polystyrene composites. *J. Mater. Res.* **2006**, *21*, 2794–2800. [[CrossRef](#)]
40. Zhi, C.; Bando, Y.; Tang, C.; Kuwahara, H.; Golberg, D. Large-scale fabrication of boron nitride nanosheets and their utilization in polymeric composites with improved thermal and mechanical properties. *Adv. Mater.* **2009**, *21*, 2889–2893. [[CrossRef](#)]
41. Coleman, J.N.; Lotya, M.; O’Neill, A.; Bergin, S.D.; King, P.J.; Khan, U.; Young, K.; Gaucher, A.; De, S.; Smith, R.J. Two-dimensional nanosheets produced by liquid exfoliation of layered materials. *Science* **2011**, *331*, 568–571. [[CrossRef](#)]
42. Wang, X.; Zhi, C.; Li, L.; Zeng, H.; Li, C.; Mitome, M.; Golberg, D.; Bando, Y. “Chemical blowing” of thin-walled bubbles: High-throughput fabrication of large-area, few-layered BN and Cx-BN nanosheets. *Adv. Mater.* **2011**, *23*, 4072–4076. [[CrossRef](#)]
43. Zhi, C.; Bando, Y.; Terao, T.; Tang, C.; Kuwahara, H.; Golberg, D. Chemically activated boron nitride nanotubes. *Chem. Asian J.* **2009**, *4*, 1536–1540. [[CrossRef](#)]
44. Andrew, E.; Kidambi, P.R. A Review of scalable hexagonal boron nitride (h-BN) synthesis for present and future applications. *Adv. Mater.* **2023**, *35*, 2207374.
45. Shim, J.; Kostecki, R.; Richardson, T.; Song, X.; Striebel, K.A. Electrochemical analysis for cycle performance and capacity fading of a lithium-ion battery cycled at elevated temperature. *J. Power Sources* **2002**, *112*, 222–230. [[CrossRef](#)]
46. Kang, J.; Rizzoni, G. Study of relationship between temperature and thermal energy, operating conditions as well as environmental factors in large-scale lithium-ion batteries. *Int. J. Energy Res.* **2014**, *38*, 1994–2002. [[CrossRef](#)]
47. Lewandowski, A.; Świderska-Mocek, A. Ionic liquids as electrolytes for Li-ion batteries—An overview of electrochemical studies. *J. Power Sources* **2009**, *194*, 601–609. [[CrossRef](#)]
48. Wang, Y.; Zaghib, K.; Guerfi, A.; Bazito, F.F.; Torresi, R.M.; Dahn, J. Accelerating rate calorimetry studies of the reactions between ionic liquids and charged lithium ion battery electrode materials. *Electrochim. Acta* **2007**, *52*, 6346–6352. [[CrossRef](#)]
49. Lux, S.F.; Schmuck, M.; Jeong, S.; Passerini, S.; Winter, M.; Balducci, A. Li-ion anodes in air-stable and hydrophobic ionic liquid-based electrolyte for safer and greener batteries. *Int. J. Energy Res.* **2010**, *34*, 97–106. [[CrossRef](#)]
50. MacFarlane, D.R.; Tachikawa, N.; Forsyth, M.; Pringle, J.M.; Howlett, P.C.; Elliott, G.D.; Davis, J.H.; Watanabe, M.; Simon, P.; Angell, C.A. Energy applications of ionic liquids. *Energy Environ. Sci.* **2014**, *7*, 232–250. [[CrossRef](#)]
51. Rodrigues, M.T.F.; Kalaga, K.; Gullapalli, H.; Babu, G.; Reddy, A.L.M.; Ajayan, P.M. Hexagonal Boron Nitride-Based Electrolyte Composite for Li-Ion Battery Operation from Room Temperature to 150 °C. *Adv. Energy Mater.* **2016**, *6*, 1600218. [[CrossRef](#)]
52. Kim, D.; Liu, X.; Yu, B.; Mateti, S.; O’Dell, L.A.; Rong, Q.; Chen, Y. Amine-functionalized boron nitride nanosheets: A new functional additive for robust, flexible ion gel electrolyte with high lithium-ion transference number. *Adv. Funct. Mater.* **2020**, *30*, 1910813. [[CrossRef](#)]
53. Arora, P.; Zhang, Z. Battery separators. *Chem. Rev.* **2004**, *104*, 4419–4462. [[CrossRef](#)] [[PubMed](#)]
54. Zhang, X.; Ji, L.; Toprakci, O.; Liang, Y.; Alcoutlabi, M. Electrospun nanofiber-based anodes, cathodes, and separators for advanced lithium-ion batteries. *Polym. Rev.* **2011**, *51*, 239–264. [[CrossRef](#)]
55. Wu, H.; Zhuo, D.; Kong, D.; Cui, Y. Improving battery safety by early detection of internal shorting with a bifunctional separator. *Nat. Commun.* **2014**, *5*, 5193. [[CrossRef](#)]
56. Luo, W.; Zhou, L.; Fu, K.; Yang, Z.; Wan, J.; Manno, M.; Yao, Y.; Zhu, H.; Yang, B.; Hu, L. A thermally conductive separator for stable Li metal anodes. *Nano Lett.* **2015**, *15*, 6149–6154. [[CrossRef](#)]
57. De Moraes, A.C.; Hyun, W.J.; Luu, N.S.; Lim, J.-M.; Park, K.-Y.; Hersam, M.C. Phase-inversion polymer composite separators based on hexagonal boron nitride nanosheets for high-temperature lithium-ion batteries. *ACS Appl. Mater. Interfaces* **2020**, *12*, 8107–8114. [[CrossRef](#)]
58. Han, R.; Liu, F.; Wang, X.; Huang, M.; Li, W.; Yamauchi, Y.; Sun, X.; Huang, Z. Functionalised hexagonal boron nitride for energy conversion and storage. *J. Mater. Chem. A* **2020**, *8*, 14384–14399. [[CrossRef](#)]
59. Zhang, J.; Zhang, Y.-F.; Huang, S.-P.; Lin, W.; Chen, W.-K. BC₂N/graphene heterostructure as a promising anode material for rechargeable Li-ion batteries by density functional calculations. *J. Phys. Chem. C* **2019**, *123*, 30809–30818. [[CrossRef](#)]
60. Lei, W.; Qin, S.; Liu, D.; Portehault, D.; Liu, Z.; Chen, Y. Large scale boron carbon nitride nanosheets with enhanced lithium storage capabilities. *Chem. Commun.* **2013**, *49*, 352–354. [[CrossRef](#)]
61. David, L.; Bernard, S.; Gervais, C.; Miele, P.; Singh, G. Facile synthesis and high rate capability of silicon carbonitride/boron nitride composite with a sheet-like morphology. *J. Phys. Chem. C* **2015**, *119*, 2783–2791. [[CrossRef](#)]
62. Ergen, O. Hexagonal boron nitride incorporation to achieve high performance Li₄Ti₅O₁₂ electrodes. *AIP Adv.* **2020**, *10*, 045040. [[CrossRef](#)]
63. Mussa, Y.; Ahmed, F.; Arsalan, M.; Alsharaeh, E. Two dimensional (2D) reduced graphene oxide (RGO)/hexagonal boron nitride (h-BN) based nanocomposites as anodes for high temperature rechargeable lithium-ion batteries. *Sci. Rep.* **2020**, *10*, 1882. [[CrossRef](#)] [[PubMed](#)]
64. Nejati, K.; Hosseiniyan, A.; Edjlali, L.; Vessally, E. The effect of structural curvature on the cell voltage of BN nanotube based Na-ion batteries. *J. Mol. Liq.* **2017**, *229*, 167–171. [[CrossRef](#)]
65. Hosseiniyan, A.; Soleimani-Amiri, S.; Arshadi, S.; Vessally, E.; Edjlali, L. Boosting the adsorption performance of BN nanosheet as an anode of Na-ion batteries: DFT studies. *Phys. Lett. A* **2017**, *381*, 2010–2015. [[CrossRef](#)]
66. Shukla, V.; Araujo, R.B.; Jena, N.K.; Ahuja, R. The curious case of two dimensional Si₂BN: A high-capacity battery anode material. *Nano Energy* **2017**, *41*, 251–260. [[CrossRef](#)]

67. Bao, J.; Zhu, L.; Wang, H.; Han, S.; Jin, Y.; Zhao, G.; Zhu, Y.; Guo, X.; Hou, J.; Yin, H. Hexagonal boron nitride/blue phosphorene heterostructure as a promising anode material for Li/Na-ion batteries. *J. Phys. Chem. C* **2018**, *122*, 23329–23335. [[CrossRef](#)]
68. Manthiram, A.; Fu, Y.; Su, Y. Sulfur-lithium-insertion compound composite cathodes for Li-S batteries. *Acc. Chem. Res.* **2013**, *46*, 1125–1134. [[CrossRef](#)]
69. Cheon, S.-E.; Ko, K.-S.; Cho, J.-H.; Kim, S.-W.; Chin, E.-Y.; Kim, H.-T. Rechargeable lithium sulfur battery: I. Structural change of sulfur cathode during discharge and charge. *J. Electrochem. Soc.* **2003**, *150*, A796. [[CrossRef](#)]
70. Mikhaylik, Y.V.; Akridge, J.R. Polysulfide shuttle study in the Li/S battery system. *J. Electrochem. Soc.* **2004**, *151*, A1969. [[CrossRef](#)]
71. Huang, J.-Q.; Zhuang, T.-Z.; Zhang, Q.; Peng, H.-J.; Chen, C.-M.; Wei, F. Permselective graphene oxide membrane for highly stable and anti-self-discharge lithium-sulfur batteries. *ACS Nano* **2015**, *9*, 3002–3011. [[CrossRef](#)] [[PubMed](#)]
72. Liang, S.; Yang, H.; Yang, H.; Tao, B.; Djeffal, A.; Chshiev, M.; Huang, W.; Li, X.; Ferri, A.; Desfeux, R. Ferroelectric control of organic/ferromagnetic spininterface. *Adv. Mater.* **2016**, *28*, 10204–10210. [[CrossRef](#)]
73. Bai, S.; Liu, X.; Zhu, K.; Wu, S.; Zhou, H. Metal-organic framework-based separator for lithium-sulfur batteries. *Nat. Energy* **2016**, *1*, 16094. [[CrossRef](#)]
74. Zhang, Z.; Lai, Y.; Zhang, Z.; Zhang, K.; Li, J. Al₂O₃-coated porous separator for enhanced electrochemical performance of lithium sulfur batteries. *Electrochim. Acta* **2014**, *129*, 55–61. [[CrossRef](#)]
75. Xu, G.; Yan, Q.-b.; Wang, S.; Kushima, A.; Bai, P.; Liu, K.; Zhang, X.; Tang, Z.; Li, J. A thin multifunctional coating on a separator improves the cyclability and safety of lithium sulfur batteries. *Chem. Sci.* **2017**, *8*, 6619–6625. [[CrossRef](#)] [[PubMed](#)]
76. Kim, P.J.H.; Seo, J.; Fu, K.; Choi, J.; Liu, Z.; Kwon, J.; Hu, L.; Paik, U. Synergistic protective effect of a BN-carbon separator for highly stable lithium sulfur batteries. *NPG Asia Mater.* **2017**, *9*, e375. [[CrossRef](#)]
77. Fan, Y.; Liu, D.; Rahman, M.M.; Tao, T.; Lei, W.; Mateti, S.; Yu, B.; Wang, J.; Yang, C.; Chen, Y. Repelling polysulfide ions by boron nitride nanosheet coated separators in lithium-sulfur batteries. *ACS Appl. Energy Mater.* **2019**, *2*, 2620–2628. [[CrossRef](#)]
78. Kim, H.-S.; Kang, H.-J.; Lim, H.; Hwang, H.J.; Park, J.-W.; Lee, T.-G.; Cho, S.Y.; Jang, S.G.; Jun, Y.-S. Boron Nitride Nanotube-Based Separator for High-Performance Lithium-Sulfur Batteries. *Nanomaterials* **2021**, *12*, 11. [[CrossRef](#)]
79. Tao, T.; Lu, S.; Fan, Y.; Lei, W.; Huang, S.; Chen, Y. Anode improvement in rechargeable lithium-sulfur batteries. *Adv. Mater.* **2017**, *29*, 1700542. [[CrossRef](#)]
80. Fan, Y.; Yang, Z.; Hua, W.; Liu, D.; Tao, T.; Rahman, M.M.; Lei, W.; Huang, S.; Chen, Y. Functionalized Boron Nitride Nanosheets/Graphene Interlayer for Fast and Long-Life Lithium-Sulfur Batteries. *Adv. Energy Mater.* **2017**, *7*, 1602380. [[CrossRef](#)]
81. Yu, B.; Fan, Y.; Mateti, S.; Kim, D.; Zhao, C.; Lu, S.; Liu, X.; Rong, Q.; Tao, T.; Tanwar, K.K. An Ultra-Long-Life Flexible Lithium-Sulfur Battery with Lithium Cloth Anode and Polysulfone-Functionalized Separator. *ACS Nano* **2020**, *15*, 1358–1369. [[CrossRef](#)] [[PubMed](#)]
82. Cheng, Q.; Li, A.; Li, N.; Li, S.; Zangiabadi, A.; Huang, W.; Li, A.C.; Jin, T.; Song, Q.; Xu, W. Stabilizing solid electrolyte-anode interface in Li-metal batteries by boron nitride-based nanocomposite coating. *Joule* **2019**, *3*, 1510–1522. [[CrossRef](#)]
83. Ji, L.; Rao, M.; Zheng, H.; Zhang, L.; Li, Y.; Duan, W.; Guo, J.; Cairns, E.J.; Zhang, Y. Graphene oxide as a sulfur immobilizer in high performance lithium/sulfur cells. *J. Am. Chem. Soc.* **2011**, *133*, 18522–18525. [[CrossRef](#)] [[PubMed](#)]
84. Liu, D.; Zhang, C.; Lv, X.; Zheng, X.; Zhang, L.; Zhi, L.; Yang, Q.H. Spatially Interlinked Graphene with Uniformly Loaded Sulfur for High Performance Li-S Batteries. *Chin. J. Chem.* **2016**, *34*, 41–45. [[CrossRef](#)]
85. Niu, S.; Lv, W.; Zhang, C.; Li, F.; Tang, L.; He, Y.; Li, B.; Yang, Q.-H.; Kang, F. A carbon sandwich electrode with graphene filling coated by N-doped porous carbon layers for lithium-sulfur batteries. *J. Mater. Chem. A* **2015**, *3*, 20218–20224. [[CrossRef](#)]
86. Xin, S.; Gu, L.; Zhao, N.-H.; Yin, Y.-X.; Zhou, L.-J.; Guo, Y.-G.; Wan, L.-J. Smaller sulfur molecules promise better lithium-sulfur batteries. *J. Am. Chem. Soc.* **2012**, *134*, 18510–18513. [[CrossRef](#)] [[PubMed](#)]
87. Yu, M.; Li, R.; Wu, M.; Shi, G. Graphene materials for lithium-sulfur batteries. *Energy Storage Mater.* **2015**, *1*, 51–73. [[CrossRef](#)]
88. Yan, X.; Jia, Y.; Chen, J.; Zhu, Z.; Yao, X. Defective-activated-carbon-supported Mn-Co nanoparticles as a highly efficient electrocatalyst for oxygen reduction. *Adv. Mater.* **2016**, *28*, 8771–8778. [[CrossRef](#)]
89. Li, M.; Fu, K.; Wang, Z.; Cao, C.; Yang, J.; Zhai, Q.; Zhou, Z.; Ji, J.; Xue, Y.; Tang, C. Enhanced Adsorption of Polysulfides on Carbon Nanotubes/Boron Nitride Fibers for High-Performance Lithium-Sulfur Batteries. *Chem. A Eur. J.* **2020**, *26*, 17567–17573. [[CrossRef](#)]
90. Sun, C.; Hai, C.; Zhou, Y.; Shen, Y.; Li, X.; Sun, Y.; Zhang, G.; Zeng, J.; Dong, S.; Ren, X. Highly Catalytic Boron Nitride Nanofiber In Situ Grown on Pretreated Ketjenblack as a Cathode for Enhanced Performance of Lithium-Sulfur Batteries. *ACS Appl. Energy Mater.* **2020**, *3*, 10841–10853. [[CrossRef](#)]
91. Mussa, Y.; Bayhan, Z.; Althubaiti, N.; Arsalan, M.; Alsharaeh, E. Hexagonal boron nitride effect on the performance of graphene-based lithium-sulfur batteries and its stability at elevated temperatures. *Mater. Chem. Phys.* **2021**, *257*, 123807. [[CrossRef](#)]

Disclaimer/Publisher’s Note: The statements, opinions and data contained in all publications are solely those of the individual author(s) and contributor(s) and not of MDPI and/or the editor(s). MDPI and/or the editor(s) disclaim responsibility for any injury to people or property resulting from any ideas, methods, instructions or products referred to in the content.